First publ. in: Macromolecules 30 (1997), pp. 5133-5155

Polymer-Mode-Coupling Theory of Finite-Size-Fluctuation Effects in Entangled Solutions, Melts, and Gels. 1. General Formulation and Predictions

Matthias Fuchs[†] and Kenneth S. Schweizer*

Departments of Materials Science and Engineering and Chemistry and Materials Research Laboratory, University of Illinois, 1304 West Green Street, Urbana, Illinois 61801

Received February 20, 1997[⊗]

ABSTRACT: The transport coefficients of dense polymeric fluids are approximately calculated from the microscopic intermolecular forces. The following finite molecular weight effects are discussed within the polymer-mode-coupling theory (PMC) and compared to the corresponding reptation/tube ideas: constraint release mechanism, spatial inhomogeneity of the entanglement constraints, and tracer polymer shape fluctuations. The entanglement corrections to the single polymer Rouse dynamics are shown to depend on molecular weight via the ratio N/N_e, where the entanglement degree of polymerization, N_e, can be measured from the plateau shear modulus. Two microscopically defined nonuniversal parameters, an entanglement strength $1/\alpha$, and a length scale ratio, $\delta = \xi_\rho/b$, where ξ_ρ and b are the density screening and entanglement length, respectively, are shown to determine the reduction of the entanglement effects relative to the reptation-like asymptotes of PMC theory. Large finite size effects are predicted for reduced degrees of polymerization up to $N/N_e \leq 10^3$. Effective power law variations for intermediate N/N_e of the viscosity, $\eta \sim N^x$, and the diffusion constant, $D \sim N^{-y}$, can be explained with exponents significantly exceeding the asymptotic values, $x \geq 3$ and $y \geq 2$, respectively. Extensions of the theory to treat tracer dielectric relaxation, and polymer transport in gels and other amorphous systems, are also presented.

1. Introduction

The transport properties of long chain polymers show characteristic phenomena attributed to chain "entanglements".[1−3] As these effects are specific to macromolecules, they appear connected to the internal degrees of freedom of the polymers. The reptation/tube theory has developed an approach to the problem of entanglements of flexible chain polymers, which has proved very versatile and has found widespread use.[2−4] Essential for this approach is the postulate of a phenomenological concept, the confining "tube" and anisotropic reptative motion of a polymer in the tube.

Recently, a microscopic theoretical approach has been formulated by one of us.[5,6] It starts from approximations to the exact expressions for the microscopic forces and attempts to derive the dynamics of entangled polymers from the underlying equilibrium structure of the polymeric liquid. The connection of both theories has not been worked out comprehensively, as the theoretical descriptions and some of the involved approximations strongly differ. However, for linear chains in 3-dimensions both theoretical approaches arrive at identical predictions for the exponents characterizing the asymptotic scaling of the transport properties with molecular weight.

It is well documented that experimental studies of entangled polymeric melts and solutions find only partial agreement of predicted and measured exponents.[1,7] Especially, the long standing issue of the dependence of the shear viscosity on molecular weight should be mentioned; experimentally $\eta \sim M^{3.4\pm0.2}$ is observed,[1] whereas both theories predict $\eta \sim M^3$ asymptotically. Moreover, recent experiments on entangled polymer solutions,[8−10] and diffusion of polymer tracer chains in cross-linked gels,[11,12] find strong deviations from the theoretical predictions for the diffusion coefficients, $D \sim M^{-2}$. Larger exponents, e.g., $D \sim M^{-2.8}$, are reported in gels,[11] and solutions, whereas in polymer melts the predicted exponents apparently describe the limiting behavior to within experimental error.[13] At present, the findings in gels and solutions cannot be rationalized within the reptation theory,[14] even including nonasymptotic corrections resulting from the finite size of the tracer or matrix polymers.[15−19] Another set of recent intriguing experiments are the measurements of the dielectric relaxation times of tracer polymers in highly entangled polymeric melts.[20,21] Depending on the matrix molecular weight, Rouse, $\tau \sim M^2$, reptation-like scaling, $\tau \sim M^3$, or power law scaling with exponents between 2 and 3 is observed. In all cases, except for the Rouse limit, however, the distribution of relaxation rates characterizing the dielectric disentanglement process is much broader than expected from the reptation results for the tube survival function.[3]

In this paper we study whether the recent polymer mode coupling (PMC) theory,[5,6] which recovers the scalings, $\eta \sim N^3$ and $D \sim N^{-2}$, in the asymptotic regime, can account for the observed different molecular weight dependences for finite N. In particular, the PMC description of the constraint release mechanism and the constraint porosity corrections are analyzed within a simplified model for polymer liquids. Our goal is a unified understanding of *all* the puzzling nonasymptotic behaviors, for tracer diffusion and self-diffusion and chain relaxation in solutions, melts, and gels, within a single theoretical framework formulated at the molecular level. Throughout this paper, extensive comparison with the reptation/tube approach is drawn in order to explain the physical content of PMC theory. Tracer dynamical shape fluctuations are also included in our study since they are the origin of power law frequency behavior in the short time asymptote of the disentanglement process in the shear modulus or the end-to-end vector correlation function.

[†] Current address: Physik-Department, Technische Universität München, D-85747 Garching, Germany.

[⊗] Abstract published in *Advance ACS Abstracts,* July 15, 1997.

In the accompanying paper,[22] the theoretical description will be tested in comparisons with various experimental data sets. A major virtue of the PMC approach, which starts from the microscopic force balance equations, is to provide connections between the dynamics and the underlying equilibrium liquid and macromolecule structure. This allows independent theoretical or experimental information to be used in order to predict the magnitudes and trends of the finite size corrections and of the asymptotic prefactors. These estimates, and discussions of both extensions of the pure reptation/tube picture to include finite size corrections and alternative nonreptation approaches to the dynamics of entangled polymers, will be included in the second paper.

The contents of this paper is as follows. Section 2 presents those aspects of the theory that are required for the present discussion and a careful enumeration of the necessary approximations. A new derivation of PMC theory based on the collective shear stress field as a primary slow variable is also presented. In section 3, the origins of finite size effects within the PMC approach are discussed, and simple models for their description are introduced. The previously obtained asymptotic predictions of PMC theory are summarized in section 4.A. Section 4.B develops the theoretical formulas including finite N corrections for the diffusion constants, viscosities, and the internal and end-to-end-vector relaxation times. In section 5, model calculations for the transport coefficients, tracer and self-diffusion constants, viscosities, and dielectric relaxation times of polymeric melts and solutions show the importance of finite size effects, and a discussion of their physical origins within the PMC description is presented. Extensions of the theory to polymer tracer diffusion through gels are presented and analyzed in section 6. The discussion in section 7 summarizes our findings and their connection to the reptation/tube approach. Finally, we note that the present and following paper are rather long. We believe this is inevitable given our goals: (i) development of a very general theory, (ii) clear explanation of the physical and mathematical content of PMC theory and its similarities and differences with respect to reptation/tube and other phenomenological approaches, and (iii) unified, comprehensive description of all nonasymptotic corrections to the transport properties of melts, solutions, and gels.

2. Theory

A. Generalized Langevin Equations. Use of the exact Mori−Zwanzig formalism allows one to derive a generalized Langevin equation for the dynamics of the segments of a tracer polymer chain in a polymeric liquid.[5] In order to proceed, knowledge of the microscopic forces acting on the tracer segments is required. The ideality concept of Flory,[23] which states that chain macromolecules in a dense, polymeric melt exhibit ideal, random-walk intramolecular correlations, simplifies the intramolecular forces. The limit of large degree of polymerization, N, of the tracer, is mathematically attractive since the discrete nature of the polymer segments can be neglected.[3,24] Then, the continuous Gaussian space curve description is generally assumed to be valid, leading to $\mathbf{F}_\alpha^{\text{intra}}(t) = K_S \partial_\alpha{}^2 \mathbf{R}_\alpha(t)$, where K_S is the entropic spring constant and $\mathbf{R}_\alpha(t)$ is the position vector of segment α on the tracer polymer. Time and segment length derivatives are abbreviated by $\partial_t = \partial/\partial t$ and $\partial_\alpha{}^2 = (\partial/\partial_\alpha)^2$, respectively. Extensions to incorporate the discrete structure of the chains or non-Gaussian intramolecular correlations, like chain stiffness, have been studied[25,26] but are neglected in the present work. Our approach, therefore, is limited to dynamical processes acting on length scales large compared to segmental sizes. Formulating this restriction as an inequality, $b \gg \sigma$ is required, where b denotes the entanglement length (to be discussed below) and σ is an effective, Gaussian-segment size determined by the persistence length of the semiflexible polymer.[23]

Far less is known about the time and space correlations of the intermolecular forces exerted by the surrounding polymeric matrix on the tracer. The rapid collective local dynamical variables, including, when appropriate, the solvent, give rise to an instantaneous, uniform friction described by the monomeric friction coefficient, ζ_0. Yet unspecified, slow collective degrees of freedom lead to a nontrivial memory function $\Gamma_{\alpha\beta}(t)$, the autocorrelation function of the slow fluctuating intermolecular forces[5] $\mathbf{F}_\alpha^Q(t)$:

$$\zeta_0 \partial_t \mathbf{R}_\alpha(t) - K_S \partial_\alpha{}^2 \mathbf{R}_\alpha(t) + \int_0^N \mathrm{d}\beta \int_0^t \mathrm{d}t'\, \Gamma_{\alpha\beta}(t-t')\, \partial_{t'} \mathbf{R}_\beta(t') = \mathbf{F}_\alpha^Q(t) \quad (1)$$

$$K_S = \frac{3k_B T}{\sigma^2} \quad (2)$$

$$\Gamma_{\alpha\beta}(t) = \frac{1}{3k_B T} \langle \mathbf{F}_\alpha^Q(t) \cdot \mathbf{F}_\beta(0) \rangle \qquad \text{where}$$

$$\langle \mathbf{F}_\alpha^Q(t) \cdot \mathbf{R}_\beta(0) \rangle = 0 \quad (3)$$

In eqs 1 and 3 the possible spatial anisotropy of the intermolecular forces on the segment size length scale is neglected, and a spatially isotropic motion is assumed.[5,27] Whether such an isotropic description is literally valid or represents a kind of effective medium description of cage-averaged dynamics, remains unresolved. The topology of linear chains determines the boundary condition of vanishing distortion at the free chain ends:[3,24]

$$\partial_\alpha \mathbf{R}_\alpha(t) = 0 \qquad \text{for} \qquad \alpha = 0, N \quad (4)$$

The initial values or equilibrium correlations again follow from the ideal Gaussian intramolecular structure:[3,23]

$$\langle (\mathbf{R}_\alpha(0) - \mathbf{R}_\beta(0))^2 \rangle = \sigma^2 |\alpha - \beta| \quad (5)$$

Special effects of semiflexibility are neglected here and eq 5 defines the effective segment size σ.

These equations have been solved and their physical predictions have been discussed by Schweizer and coworkers within the PMC theory based on various approximations.[5,6,28−34] In the present paper we will improve upon one of the approximations, namely the frozen matrix assumption,[5] in order to study the consequences on the probe dynamics of taking into account more realistically the dynamics of the surrounding medium. We consider the tracer to be embedded in a liquid of ν, chemically identical chain polymers of degree of polymerization P. The polymer segment density, ρ_m, therefore is $\rho_m = P\nu/V$.

The tracer diffusion coefficient is defined in the usual manner from the motion of the center-of-mass, $\mathbf{R}^{\text{CM}}(t)$

$= N^{-1}\int_0^N \mathrm{d}\alpha\ \mathbf{R}_\alpha(t)$, in the hydrodynamic, or long time, limit:[3,35]

$$\langle(\mathbf{R}^{\mathrm{CM}}(t) - \mathbf{R}^{\mathrm{CM}}(0))^2\rangle \to 6Dt \qquad \text{for} \qquad t \to \infty \quad (6)$$

From the previous analysis of the PMC equations it is known that they describe a dynamical process that has been favorably compared to the entanglement dynamics as measured by diffusion experiments, rheology, pulsed field gradient NMR, and dielectric spectroscopy.[30,31,33,34,36] The theory predicts the existence of a strongly N dependent terminal or disentanglement time, τ_{D}, which in the present context can be defined by the final relaxation step in the internal, conformational dynamics of the tracer polymer:[6]

$$\langle\mathbf{F}_\alpha^{\mathrm{intra}}(t)\cdot\mathbf{F}_\beta^{\mathrm{intra}}(0)\rangle \to \langle\mathbf{F}_\alpha^{\mathrm{intra}}(0)\cdot\mathbf{F}_\beta^{\mathrm{intra}}(0)\rangle \mathrm{e}^{-t/2\tau_{\mathrm{D}}} \qquad \text{for} \qquad N \to \infty \quad (7)$$

Note that eq 7 holds for long times only (Markov regime). It is simplified in so far as the cutoff of the PMC effects below a certain entanglement length scale, b, is not denoted explicitly, and also small corrections to the global modes are neglected.[6,31,34] The theory also predicts the existence of an entanglement plateau, $G_N = \rho_m k_{\mathrm{B}}T/N_{\mathrm{e}}$, in the shear modulus on intermediate times.[6] (The theoretical predictions for N_{e} are quoted below.) This result depends on the generally accepted, but rigorously unverified, assumption that the measured collective shear stress is dominated by the incoherently added, single chain contributions.[3,37] From this amplitude of the entanglement process in the shear stress, G_{N}, and the final relaxation time τ_{D} of eq 7, follows the shear viscosity:[6,31]

$$\eta = G_N\tau_{\mathrm{D}} + \eta^{\mathrm{R}} = \frac{\rho_m k_{\mathrm{B}}T}{N_{\mathrm{e}}}\tau_{\mathrm{D}} + \eta^{\mathrm{R}} \quad (8)$$

In eq 8, a simple additivity assumption was used in order to describe the crossover from the low molecular weight, Rouse[3,24] result, $\eta^{\mathrm{R}} = \rho_m\zeta_0\sigma^2N/36$, to the high molecular weight, asymptotic PMC result, $\eta^{\mathrm{PMC}} = G_N\tau_{\mathrm{D}}$. This assumption is expected to be reliable at rather high molecular weights and compares well with numerical solutions to the full PMC equations including crossover effects.[31]

The calculation of the tracer diffusion coefficient, D, and the internal final relaxation time, τ_{D}, can proceed from the exact starting equations (1)−(5) only via approximations. Calculating the diffusion coefficient is somewhat complicated by the coupling of translational and rotational motions as captured in eq 1 in general. (See below for a further discussion of this point.) Following previous analysis we will neglect this coupling, which arises from the end monomers of the tracer polymer, i.e., the boundary condition, eq 4, appropriate for linear chains. Naturally, it is also absent for cyclic polymers. We argue that the diffusion over distances large compared to the size of the polymer, $\Delta r \gg R_{\mathrm{g}} = \sigma\sqrt{N/6}$, is determined by the sum of all intermolecular forces acting uniformly on the center-of-mass of the probe.[34] Then the diffusion coefficient is determined from the memory function of the sum of all intermolecular forces. Reassuringly, the result for D that we will get is a clear extension of known expressions for the diffusion coefficients of atomic or colloidal systems.[35,38]

The dynamics of the uniform friction exerted on the center-of-mass is unknown and can only be found with approximations. In the approach put forward in refs 5 and 6, the uncontrolled but often surprisingly successful mode-coupling approximation[5,35,39−43] is used. It requires a physically motivated choice of the relevant, slow modes. We assume that the dynamics of the center-of-mass friction is dominated by the collective density fluctuations of the matrix, $c_{\mathbf{k}}(t)$,

$$c_{\mathbf{k}}(t) = \sum_{m=1}^{\nu}\int_0^P \mathrm{d}\gamma\ \mathrm{e}^{i\mathbf{k}\mathbf{R}_\gamma^m(t)} \quad (9)$$

and the collective monomer density of the tracer

$$\rho_{\mathbf{k}}(t) = \int_0^N \mathrm{d}\alpha\ \mathrm{e}^{i\mathbf{k}\mathbf{R}_\alpha(t)} \quad (10)$$

In eq 9 the time dependent vector $\mathbf{R}_\gamma^m(t)$ is the position vector of segment γ on matrix polymer m. The total intermolecular fluctuating forces exerted on the tracer center-of-mass are therefore described by a memory function $\Sigma(t)$ of the form[6,34]

$$\Sigma(t) = \frac{1}{3\zeta_0 k_{\mathrm{B}}TN}\int_0^N \mathrm{d}\alpha\ \mathrm{d}\beta\ \langle\mathbf{F}_\alpha^Q(t)\cdot\mathbf{F}_\beta(0)\rangle \approx \frac{Vk_{\mathrm{B}}T}{3\zeta_0 N}\int\frac{\mathrm{d}^3\mathbf{k}}{(2\pi)^3}|\mathbf{k}V_k^{\mathrm{eff}}|^2\langle c_{-\mathbf{k}}^Q(t)\ \rho_{\mathbf{k}}^Q(t)\ c_{\mathbf{k}}^Q\rho_{-\mathbf{k}}^Q\rangle \quad (11)$$

where V is the volume, and the approximation results from assuming that the four-point correlation function of the fluctuating forces is dominated by its overlap with the correlator of the pair variables $\rho_{-\mathbf{k}}(t)\ c_{\mathbf{k}}(t)$. The label Q indicates that the projected dynamics controls the time evolution of the fluctuating forces. The projector Q formally achieves that there is no further, linear coupling of the monomer coordinates to the fluctuating forces besides the one described explicitly[35,41] in eq 1. The vertex, i.e., the normalized overlap of the forces with the slow pair variables, can be calculated[5] (when neglecting three point correlations, i.e., $Q = 1$):

$$\mathbf{k}V_k^{\mathrm{eff}} = \frac{1}{NP\nu k_{\mathrm{B}}T}\int_0^N \mathrm{d}\alpha\ \mathrm{d}\beta\ \frac{\langle c_{-\mathbf{k}}\rho_{\mathbf{k}}^\beta\mathbf{F}_\alpha^Q\rangle}{\omega_k S_k} = \frac{-i\mathbf{k}\rho_m h_k}{P\nu\omega_k S_k} \qquad \text{for} \qquad Q = 1 \quad (12)$$

It is the normalized equilibrium correlation of a collective tracer variable, $\int_0^N \mathrm{d}\alpha\ \mathbf{F}_\alpha^Q$, with the product of a collective matrix variable, $c_{\mathbf{k}}$, and another collective tracer variable, $\int_0^N \mathrm{d}\alpha\ \rho_{\mathbf{k}}^\alpha$. Therefore, it is natural that the total intermolecular correlation function, h_k, arises. This aspect also holds for atomic and colloidal systems.[38,42] Whereas the collective intramolecular structure factor, $\omega_k = N^{-1}\langle\rho_{-\mathbf{k}}(0)\ \rho_{\mathbf{k}}(0)\rangle$, describes a single polymer, the total intermolecular correlation function, $h(r) = h_{\alpha\beta}(r) = g_{\alpha\beta}(r) - 1$, is an interchain site−site radial distribution function correlating segments on different macromolecules. A peculiarity of polymeric tracers is the long-ranged spatial dependence of $h(r)$ due to the well-known correlation hole[2] effect, $h(r) \sim (-1/r)\mathrm{e}^{-r\sqrt{2}/R_{\mathrm{g}}}$ for $r \gg \sigma$. The existence of this long-ranged correlation can be argued on general grounds as a universal consequence of chain connectivity and interchain excluded volume forces. This correlation extends to the tracer size, R_{g}. Note that if the liquid is taken as a random continuum, $g(r) = 1$, then $h_k \to 0$ and all

entanglement effects vanish. In the polymer reference interaction site model (PRISM) of Curro and Schweizer, the correlation hole is rigorously recovered, but also the local structure is described realistically.[44−46] This is necessary in the present context as the short-ranged excluded volume interactions dominate the polymer liquid structure and also determine the magnitude of the entanglement friction. PRISM therefore has been used to calculate the equilibrium structural correlation functions entering into the vertices.[5,6,30−34] PRISM theory connects h_k to the intramolecular and collective structure factors, ω_k and S_k, respectively, where $S_k = \omega_k + \rho_m h_k$, and to an effective short-ranged pseudopotential, c_k, the site−site direct correlation function.

$$h_k = c_k \omega_k S_k \tag{13}$$

Although the vertex is now known, the dynamics of the projected pair variables, $\rho^Q_{-\mathbf{k}}(t)\, c^Q_{\mathbf{k}}(t)$, is not. The approach put forward by Schweizer[5,6] uses the mode factorization approximation to break the average on the right hand side of eq 11 and interprets the projected single chain dynamics of the tracer as the one arising from a perturbative short time theory, the renormalized Rouse (RR) model (see section 2.B below), and the projected collective matrix dynamics as the full entangled dynamics.

$$\langle c^Q_{-\mathbf{k}}(t)\, \rho^Q_{\mathbf{k}}(t)\, c^Q_{\mathbf{k}} \rho^Q_{-\mathbf{k}} \rangle \approx P\nu N \omega_k^{\mathrm{RR}}(t)\, S_k(t) \tag{14}$$

Even though the intermolecular site−site correlation function, h_k, is long ranged, in the final result for $\Sigma(t)$ the vertex of eq 12 is relatively short ranged because of the anticorrelated normalization of the projector.

$$\Sigma(t) \approx \frac{k_B T \rho_m}{3\zeta_0} \int \frac{\mathrm{d}^3 k}{(2\pi)^3}\, k^2 c_{\mathbf{k}}{}^2 \omega_k^{\mathrm{RR}}(t)\, S_k(t) \tag{15}$$

Equation 15 expresses that the major contributions to the $t = 0$ amplitudes of the friction (fluctuating forces) exerted on the tagged polymer center-of-mass arise from short-ranged, local intermolecular correlations. This can be seen from the wavevector dependence of the friction contributions in eq 15. Wavevectors large compared to $1/R_g$, corresponding to local distances, are weighted most heavily as $k^4\omega_k$ increases monotonically with k. However, $kR_g \leq 1$ long wavelength contributions still play a crucial role in establishing the total Markovian friction due to their long relaxation times. Figure 1 shows a schematic representation of the collective and intramolecular correlations and length scales that determine $\Sigma(t)$. The tracer interacts with the matrix polymers via the short-ranged, effective potential, $c_{\mathbf{k}}$, the direct correlation function. The spatial correlations of the fluctuating, intermolecular forces further propagate along the tracer and through the matrix medium. Intramolecular correlations along the tracer polymer are described by ω_k and are characterized by two length scales, σ (local) and R_g (global). The density screening length, ξ_ρ, and the entanglement length, b, characterize the constraining equilibrium and dynamic structure of the surrounding matrix, respectively.

The diffusion coefficient, D, can now be found in the Markovian, long time limit of eq 6,

$$D^{-1} = \frac{\zeta_0 N}{k_B T}[1 + \hat{\Sigma}_0] = \frac{\zeta_0 N}{k_B T}[1 + \int_0^\infty \mathrm{d}t\, \Sigma(t)] \tag{16}$$

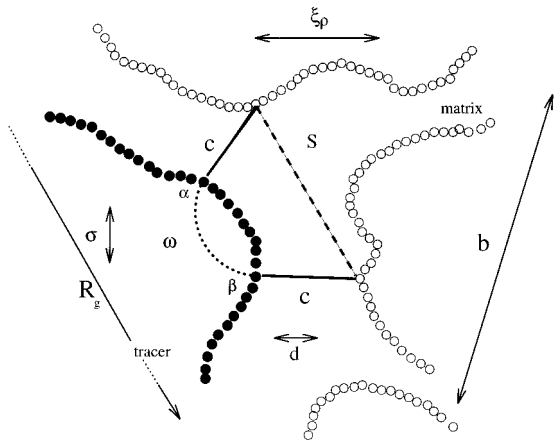

Figure 1. Schematic representation of the (static) entanglement constraints in the uniform-drag friction function, $\Sigma(t)$, eq 15, of PMC theory. The tracer, characterized by the intramolecular correlations ω and length scales σ and R_g, interacts via the short-ranged (excluded-volume diameter d) pseudopotential, c (the direct correlation function), with the matrix polymers. The entanglement constraints of the matrix separate into local (density screening length ξ_ρ) compressibility and mesoscopic (entanglement length b) elastic correlations.

Extending previous work based on an effectively static, homogeneous matrix ($S_k(t) \approx S_0$), the present study focuses on the effects of the spatial and time dependence of the matrix fluctuations, $S_k(t)$ in eq (15), on the magnitudes and the molecular weight dependences of the diffusion constant, and on other transport properties.

The calculations leading to the expressions for the internal relaxation time τ_D have been discussed in refs 6, 31, and 34. In order to show the robustness of these results, to provide further physical interpretation, and as a basis for incorporation of all finite size corrections, we rederive them arguing differently. The original aim of Kawasaki when using the mode-coupling approximation was to identify slowly varying, nonlinear contributions to the memory functions and equations of motion.[39,40,43,47] One experimentally observed slow variable in polymeric liquids is the shear stress. Its time scale, i.e., the shear disentanglement time, τ_D^s, grows strongly with molecular weight. It is the longest time scale, at least according to experimental observations, in entangled polymeric liquids not close to a demixing or order−disorder phase transition.[1−3] For example, dielectric measurements show that the internal, conformational relaxation time, τ_D^ϵ, very nearly equals τ_D^s in melts.[20] We therefore assume the existence of one disentanglement time, τ_D, appearing in different collective and single chain properties which originate in the single chain, conformational dynamics. Thus τ_D can be calculated from the disentanglement process of a (tracer) macromolecule for $N = P$ and is itself affected by the matrix disentanglement process.[6]

As τ_D is the longest relaxation time, any variable participating in the disentanglement step can be considered a slow mode. Therefore, before we summarize the theoretical or experimental evidence about the behavior of the matrix structure factor, $S_k(t)$, on this time scale, let us calculate the fluctuating force memory function, $\Gamma_{\alpha\beta}(t)$ of eq 3, assuming that it is dominated by the collective stress tensor, which is known to be slow.[1] To that end, the steps in eqs 11−15 will be repeated for those intermolecular friction forces that affect the internal conformational dynamics, replacing the collective matrix density with the collective matrix

stress tensor. Remembering that the intermolecular forces, $\mathbf{F}_\alpha(t)$, can also relax via the dynamics of a tracer segment β, a new projection of $\Gamma_{\alpha\beta}$ leads to

$$\Gamma_{\alpha\beta}(t) \approx \frac{V}{3k_BT}\sum_{abc=}^{xyz}\int\frac{d^3k}{(2\pi)^3}\int_0^N d\alpha'\, d\beta' \times V_k^{ab,\alpha\alpha'}\langle\sigma_{-\mathbf{k}}^{Qb}(t)\,\rho_{\mathbf{k}}^{Q\alpha'}(t)\,\rho_{-\mathbf{k}}^{Q\beta'}\sigma_{\mathbf{k}}^{Qc}\rangle V_k^{ca,\beta'\beta} \quad (17)$$

Here, $\sigma_k^a(t)$ is a component of the collective matrix stress tensor where one direction is longitudinal, i.e., parallel to the wavevector.

$$\boldsymbol{\sigma}_{\mathbf{k}} = -\sum_{m=1}^{\nu}\int_0^P d\gamma\,\frac{1}{k}(k_BT\mathbf{k} - i\mathbf{F}_\gamma^m)e^{i\mathbf{k}\mathbf{R}_\gamma{}^m} \quad (18)$$

The equilibrium averages of the components of the stress tensor are connected to the elastic constants or high-frequency moduli of the liquid.[35,41]

$$\langle\sigma_{-\mathbf{k}}^a\sigma_{\mathbf{k}}^b\rangle = k_BTVG_k^a\delta_{ab} \quad (19)$$

The formal expressions for the microscopic, elastic constants are known and connect G^a to the total potential including inter- and intramolecular forces.[35,41] In order to make a connection to experimental measurements, the elastic constants not at short, microscopic times but in the glass relaxation regime would be required. It is the time scale of the glassy or α-relaxation that is connected to the monomeric friction coefficient, ζ_0, entering the Rouse model and our generalization of it.[1] Except for simple liquids, little theoretical understanding of the glassy moduli exists.[42,48] Since the exact values are not required in our case, we assume for simplicity: (1) The different elements of the glassy moduli are roughly equal, $G^a \approx G$. (2) Their magnitude is $G \approx \rho_m k_BT$, as would be found in the Rouse calculation.[3] With these technical assumptions the vertices, which obey $V_k^{ab,\alpha\beta} = V_k^{a,\alpha\beta}\delta_{ab}$, simplify to $V_k^{a,\alpha\beta} = V_k^{\alpha\beta}$.

Nondiagonal elements in the memory function matrix, $\beta \neq \alpha$, arise due to the connectedness of the probe polymer and are a central element of the PMC approach. Monomer density fluctuations, $\rho_k^\alpha = e^{i\mathbf{k}\mathbf{R}_\alpha(t)}$, at different tracer sites are correlated. For a Gaussian ideal polymer the equilibrium intramolecular correlations are well-known[3] and follow from eq 5:

$$\omega_k^{\alpha\beta} = \langle e^{i\mathbf{k}(\mathbf{R}_\beta - \mathbf{R}_\alpha)}\rangle = e^{-(k^2/6)\langle(\mathbf{R}_\alpha - \mathbf{R}_\beta)^2\rangle} = e^{-(k^2\sigma^2/6)|\alpha-\beta|} \quad (20)$$

The standard normalization in the vertices, see eq 23 below, causes the appearance of the differential operator, $(\omega_k^{\alpha\beta})^{-1}$, the inverse of the "matrix" in equation 20, which is defined by

$$\int_0^N d\beta\,(\omega_k^{\alpha\beta})^{-1}\omega_k^{\beta\gamma} = \delta(\alpha-\gamma) \quad \text{and}$$
$$\partial_\alpha\omega_k^{\alpha\beta} = \pm\frac{k^2\sigma^2}{6}\omega_k^{\alpha\beta} \quad \text{for } \alpha = 0,\ N \quad (21)$$

The boundary condition simply follows from eq 4. The mathematical form of $(\omega_k^{\alpha\beta})^{-1}$ can easily be found, most simply from looking at the continuum limit of the known,[6,25] finite matrix inverse ω^{-1}.

$$(\omega_k^{\alpha\beta})^{-1} = \delta(\alpha-\beta)\left(-\frac{3}{k^2\sigma^2}\partial_\alpha{}^2 + \frac{k^2\sigma^2}{12}\right) \quad (22)$$

This leads to the following expressions for the vertices, where for simplicity the three-point correlations are neglected, i.e., $Q = 1$ in eq 23.

$$V_k^{ab,\alpha\beta} = \int_0^N d\gamma\,\langle F_\alpha^{Qa}\rho_{-\mathbf{k}}^\gamma\sigma_{\mathbf{k}}^b\rangle(\omega_k^{\gamma\beta})^{-1}\langle\sigma_{-\mathbf{k}}^b\sigma_{\mathbf{k}}^b\rangle^{-1} = -k^a\delta_{ab}\rho_m h_k\frac{k_BT}{VG_k^a}(\omega_k^{\alpha\beta})^{-1} \quad (23)$$

The approximations concerning the projector, $Q \neq 1$, and the values of the glassy moduli can easily be improved. Again, however, little is known about the dynamics of the four-point correlation function $\langle\rho^\alpha(t)\,\sigma^a(t)\,\rho^\beta\sigma^b\rangle$ in eq 17. We assume that this matrix of friction functions is dominated by exactly the same dynamical processes that determine the long time tracer diffusion coefficient. Thus, $\Gamma_{\alpha\beta}(t)$ relaxes (in a parallel fashion) via the probe motion described by the collective (coherent) single chain correlator evaluated in the renormalized Rouse model[5,6] and the full collective matrix correlator, which corresponds to the shear modulus, $G_k(t)$, for our present choice of slow variables. In this case, in order to account for the matrix structure of $\Gamma_{\alpha\beta}$, the result that adequately captures the equilibrium, $t = 0$, correlations is

$$\int_0^N d\alpha'\, d\beta'\,(\omega_k^{\alpha\alpha'})^{-1}\langle\sigma_{-\mathbf{k}}^{Qa}(t)\,\rho_{\mathbf{k}}^{Q\alpha'}(t)\,\rho_{-\mathbf{k}}^{Q\beta'}\sigma_{\mathbf{k}}^{Qb}\rangle(\omega_k^{\beta'\beta})^{-1} \approx \frac{Vk_BT}{\omega_k}G_k^a(t)\,\delta_{ab}(\omega_k^{\alpha\beta})^{-1}\,\omega_k^{RR}(t) \quad (24)$$

Before writing down the results for the friction matrix, we note that $\Gamma_{\alpha\beta}(t)$ separates into two independent memory functions because of the structure of ω^{-1}, eq 22.

$$\Gamma_{\alpha\beta}(t) = \zeta_0\delta(\alpha-\beta)(\Sigma'(t) - M(t)\partial_\alpha{}^2) \quad (25)$$

$\Sigma'(t)$ is another measure of the uniform drag exerted by the matrix on all tracer segments and is closely related to $\Sigma(t)$ of eq 15. From eqs 17−25 it follows:

$$\Sigma'(t) = \frac{(\sigma\rho_m k_BT)^2}{36\zeta_0}\int\frac{d^3k}{(2\pi)^3}\,k^4\left(\frac{h_k}{G_k}\right)^2 G_k(t)\,\frac{\omega_k^{RR}(t)}{\omega_k} \quad (26)$$

As will become evident from section 3.B, Σ and Σ' actually agree on intermediate time scales. This follows as the integrand in Σ' differs from the one in Σ, eq 15, by a factor $(\sigma^2k^2/12\omega_k)$, which equals unity for intermediate wavevectors. Σ and Σ' are identical as long as the (major) contributions to the friction of the center-of-mass arise from internal modes, i.e., from wavevectors obeying $kR_g \gg 1$. They differ somewhat for longer times because, as is evident from the different boundary conditions, the segment coordinates, $\mathbf{R}_\alpha(t)$, and the monomer densities, $\rho_k^\alpha(t)$, cannot be decomposed into the same normal modes[3,34] for finite k. This effect of the ends of the tracer chain, however, only affects the form of the final relaxation of the memory function. We prefer $\Sigma(t)$ to $\Sigma'(t)$ for both simplicity reasons, and the fact that the well-known hydrodynamic long time tail of the diffusion coefficient in colloidal systems is recovered,[34,38] $\Sigma(t) \to t^{-5/2}$ for $t \to \infty$. Very importantly, we note that the molecular weight scaling of the diffusion coefficient is *not* affected by this uncertainty about the final power law decay of the exact center-of-mass friction function.

A conceptually different friction function, $M(t)$, determines the conformational and single chain stress relaxations.[6] Equations 17−25 lead to

$$M(t) = \frac{(\rho_m k_B T)^2}{\sigma^2 \zeta_0} \int \frac{d^3k}{(2\pi)^3} \left(\frac{h_k}{G_k}\right)^2 G_k(t) \frac{\omega_k^{RR}(t)}{\omega_k} \quad (27)$$

In section 3.B the connection of eq 27 to the previously used expression[6,31] for $M(t)$ is detailed. Let us discuss the role of the conformational memory function, $M(t)$, in the long time, Markovian limit. This is possible in the asymptotic large N limit as the time scale of $M(t)$ is found[6] to be shorter than τ_D by a factor proportional to $1/\sqrt{N}$. For simplicity, let us also neglect the uniform friction contribution, i.e., $\Sigma'(t)$, and consequently study internal, conformational dynamics only. Equation 1 then reduces to

$$\zeta_0(1 - \hat{M}_0 \partial_\alpha^2)\partial_t \mathbf{R}_\alpha(t) - K_S \partial_\alpha^2 \mathbf{R}_\alpha(t) = F_\alpha^Q(t) \quad (28)$$

where

$$\hat{M}_0 = \int_0^\infty dt\, M(t) \quad (29)$$

For large $\hat{M}_0$, the disentanglement, or terminal relaxation time τ_D follows from eqs 7 and 28 and the use of Gaussian intramolecular forces:[6]

$$\tau_D = \frac{\zeta_0}{2K_S}\hat{M}_0 = \frac{\tau_0}{2}\hat{M}_0 \quad (30)$$

where $\tau_0 = \sigma^2\zeta_0/3k_BT$ connects the theoretical with the physical time. Moreover, considering eq 28 for times short compared to τ_D, one concludes that the conformational dynamics, i.e., the relaxation of the intramolecular distortions, $\partial_\alpha^2 \mathbf{R}_\alpha(t)$, is arrested up to times short compared to τ_D. The exact non-Markovian analysis of refs 6, 31, and 34 rigorizes this statement and identifies the time to be $\tau^{RR} \approx \tau_0 N^2 \sqrt{N/N_e}$. Solving the equation $\partial_\alpha^2 \mathbf{R}_\alpha(t) = \mathbf{c}_\alpha$ the only time dependence can enter via the two constants of integration. Note that they are not determined by the boundary condition, eq 4, as we are neglecting the center-of-mass motion.

$$\mathbf{R}_\alpha^{conf}(t) = \int_0^\alpha d\alpha' \left(\int_0^{\alpha'} d\alpha'' \, \mathbf{c}_{\alpha''} + \mathbf{u}(t)\right) + \mathbf{v}(t) \quad (31)$$

The entanglement process in the PMC theory leads to the prediction of a very cooperative motion of all tracer segments. Figure 2 shows this in a discrete bead−spring model, where the standard discretization of $\partial_\alpha^2 \mathbf{R}_\alpha = \mathbf{R}_{\alpha+1} - 2\mathbf{R}_\alpha + \mathbf{R}_{\alpha-1}$ applies. The restriction $\mathbf{R}_{\alpha+1} - 2\mathbf{R}_\alpha + \mathbf{R}_{\alpha-1} = 0$, where $\mathbf{c}_\alpha = 0$ is set for simplicity, constrains the conformational dynamics of the tracer for times shorter than the disentanglement time, τ_D. From the arbitrary (isotropic) displacements, **u** and **v**, of two randomly chosen segments, the motion of all other monomers is determined. The PMC theory generalizes the reptation ansatz,[2,3] that only the two end segments can move freely, to a more general, molecular architecture transcending cooperative motion; e.g., rings and chains are expected to behave very similarly. Further numerical work possibly can find information about the monomer trajectories by studying the arrested magnitudes $\mathbf{c}_\alpha$.

In summary, in the PMC approach two central memory functions describing dynamical caging of the tagged polymer by its surroundings arise in the analysis of entanglements. Assuming that the projected dynamics is dominated by the identical superposition of collective intramolecular and collective matrix structural dynamics, both memory functions are closely connected. For linear chains, in contrast to cyclic polymers, a technical complication arises from the end monomers but will be neglected as argued above and elsewhere.[6,34] The close connection of $\Sigma(t)$ and $M(t)$ immediately leads to the prediction that from eqs 15 and 27, and (reasonable) results for the collective matrix dynamics (see below), the asymptotic Stokes−Einstein ratio obeys[6,31,34]

$$\eta D/R_g^2 \sim N^0 \quad \text{for} \quad N \to \infty \quad (32)$$

This PMC prediction agrees with the reptation result and shows that the dynamics of entangled polymers differs strongly from the Rouse model,[2,3] $\eta^R D^R \sim N^0$. In this paper we will analyze finite-N corrections to D, η, and τ_D in order to study whether experimentally observed deviations from asymptotic scaling laws are described by the finite size static and/or dynamic corrections of the PMC theory.

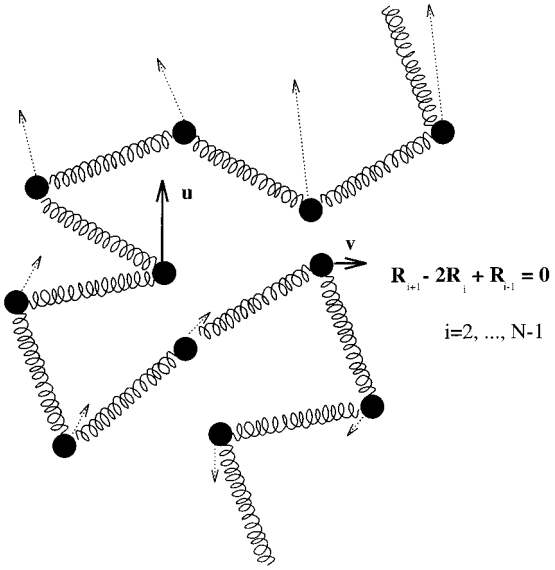

Figure 2. Schematic figure showing the restriction of the segment dynamics for times shorter than the disentanglement time. A discrete bead−spring polymer model is used, where eq 31, with the unknown $\mathbf{c}_\alpha$ set to $\mathbf{c}_\alpha = 0$ for simplicity, allows the determination of all bead displacements from the motions, **u**(**t**) and **v**(**t**), of two arbitrary segments.

B. Renormalized Rouse Model. The collective, single tracer projected dynamics entering the friction functions, $\Sigma(t)$ and $M(t)$, eqs 15 and 27, is required. Corrections to the Rouse model on short time scales have been worked out and discussed in refs 6 and 32. We will use the Markovian results of this renormalized Rouse (RR) theory, as we are interested in the transport properties of the PMC model only. In the large N limit (effectively frozen matrix), the decay of the PMC friction is dominated by the collective tracer dynamic structure factor evaluated in the RR model:[5,31]

$$\omega_k^{RR}(t) = \omega_k \exp\left[-\frac{k_B T k^2 t}{\omega_k \zeta^{RR}}\right] \quad (33)$$

where ζ^{RR} is the friction coefficient of the RR model. It results from a dynamically perturbative calculation of

the intermolecular friction and, for large N, exceeds the monomeric friction coefficient[32] ζ_0:

$$\zeta^{RR} = \zeta_0(8/27)\rho_m d^6 g_d{}^2 \int_0^\infty \mathrm{d}k\; k^2 \omega_k{}^2 S_k \rightarrow \zeta_0\sqrt{\frac{N}{N_e}} \quad \text{for} \quad N \rightarrow \infty \quad (34)$$

where, for simplicity, we drop the regular, molecular weight independent contribution (ζ_0) to ζ^{RR} and look at times long compared to the Rouse time, $\tau^R = \tau_0(N/\pi)^2$, where ζ^{RR} attains its Markovian value.[5,32] g_d is the value of the intermolecular segment−segment pair correlation function, $g(r)$, at the excluded volume diameter d, i.e., at the distance of closest approach or contact. The prefactor of the asymptotic limit, $\zeta^{RR} \sim \sqrt{N}$, defines the entanglement degree of polymerization, N_e, in the theory. It is defined to be the N where in a perturbative, crossover calculation the increase of the friction due to the slow tracer−matrix interactions equals the instantaneous friction modeled by ζ_0 in the Rouse picture.[29,32] N_e defines the crossover length scale, $b = \sigma\sqrt{N_e}$, and the Rouse mode index, $p_e = \pi/N_e$, which separates local, Rouse dynamics from the strongly entanglement affected, more collective modes. In the PMC theory the entanglement effects on local length scales are explicitly removed.[6,31] As a cutoff length or Rouse mode index the quantities b or p_e are chosen, respectively.

For later reference we quote the result for N_e following from eq 34 when setting[29,31,32,34] $\zeta^{RR}(N = N_e) = \zeta_0$:

$$N_e = [\sqrt{3}\pi(16/9)\rho_m \sigma^3 \Gamma^{-6} g_d{}^2 S_0]^{-2} \quad (35)$$

where $\Gamma = \sigma/d$ is an effective chain aspect ratio,[23,45] set equal to unity for simplicity throughout this and the following paper.

Without repeating the discussion of the RR model from refs 6 and 32, we recall that the buildup of friction is evaluated for times short compared to the dynamics of the matrix. Thus, the assumption in the RR model of a frozen matrix, $S_k(t) = S_k$, is appropriate for entangled polymeric liquids only. Extensions of the theory to the tracer dynamics in short, unentangled polymer solutions and melts require a treatment different from that presented here. The RR results, eqs 33 and 34, can be viewed as a weak coupling and short time limit to the Σ-memory function of the PMC description. Namely, the effective potential or direct correlation function is estimated from the excluded volume interactions, $c(r) = -V(r)/k_BT = -(4\pi/3)d^3 \cdot g_d\delta(r)$, and the collective dynamics of the tracer is taken from the Rouse model and is assumed to be rate determining for the fluctuating force relaxation.

3. Finite Size Effects in PMC Theory

A. Tracer Shape Fluctuations. The relaxation of the entanglement constraints and their resulting memory functions, $\Sigma(t)$ and $M(t)$, progresses via parallel dynamical processes or channels. If any of these channels were ineffective, i.e., its contribution to the friction did not relax, the entanglements could only relax via the other channels and would be slowed down. Besides the matrix relaxation, which will be discussed in the next section, the tracer dynamics as described by eq 33 opens two channels for fluctuating force relaxation. A more collective one at small wavevectors is associated with probe center-of-mass translation, and a more local decay channel at larger wavevectors that can be identified with probe shape fluctuations. The first process relaxes the fluctuating forces via the coherent motion of all tracer segments, i.e., the center-of-mass dynamics of the RR model, $\omega_k^{RR}(t) \sim N\mathrm{e}^{-(k_BTk^2t/N\zeta^{RR})}$ for $kR_g \ll 1$. Presumably, this decay channel is the PMC (isotropic) analog of a coherent (anisotropic) reptative motion. The local probe shape fluctuations for $kR_g \gg 1$ arise from the continuous spectrum of internal modes. Eq 33 approximates those with the well-known first cumulant expression advocated by Akcasu and co-workers,[49] which correctly describes the time-spatial correlations, i.e. the scaling with k^4t in the case of the Rouse model.[2,3]

The shape, or internal mode, fluctuations lead to a speeding up of the dynamical relaxation of fluctuating (entanglement) forces associated with dynamically correlated processes on length scales $\ll R_g$. It is instructive to neglect the shape fluctuation mechanism and extend the diffusive center-of-mass dynamics, $\Phi_{cm}^{RR}(t,k) = \mathrm{e}^{-(k_BTk^2t/N\zeta^{RR})}$, to arbitrary wavevectors and compare the predicted behavior with the full PMC and the reptation/tube results. In order not to vary the wavevector dependent contributions to the entanglement friction functions, this change in the decay rates has to be accompanied by an appropriate change in the entanglement amplitudes. Adopting the frozen matrix approximation for simplicity these adjustments lead, starting from eqs 15 and 27, to the following memory functions:

$$\tilde{\Sigma}(t) \propto \frac{1}{\sqrt{N_e}} \int_0^\infty \mathrm{d}k\; k^4 \frac{\omega_k{}^2}{N} \Phi_{cm}^{RR}(t,k) \quad (36)$$

$$\tilde{M}(t) \propto \frac{1}{\sqrt{N_e}} \int_0^\infty \mathrm{d}k\; k^2 \frac{\omega_k{}^3}{N} \Phi_{cm}^{RR}(t,k) \quad (37)$$

By construction, this change does not lead to changes in the asymptotic scaling of the transport coefficients but has interesting effects for the short time asymptote of the disentanglement process. Note also that the identical N-scaling for the internal dynamics, i.e., $\tilde{M}_0 \sim \hat{M}_0 \sim N^3$, would be obtained even without adjusting the entanglement amplitudes but only suppressing the shape fluctuation contribution to force relaxation. It is only in the center-of-mass fraction function, $\Sigma(t)$, eq 15, that neglecting the shape fluctuations without correcting the amplitudes would lead to a nonreptation-like Markovian result, $\hat{\Sigma}_0 \sim N^{3/2}$.

Let us recall from the reptation/tube theory that the polymer end-to-end vector correlation function, $\langle \mathbf{P}(t)\cdot\mathbf{P}(0)\rangle$, and the shear modulus, $G(t)$, are proportional to the same function $\psi(t)$, the tube survival function.[3] Therefore, they exhibit the following asymptote in the reptation theory:

$$G''(\omega)/G_N \propto \langle \mathbf{P}''(\omega)\cdot\mathbf{P}(0)\rangle/R_g{}^2 \propto (\omega\tau_0 N^3)^{-1/2} \quad \text{for} \quad \omega\tau_0 N^3 \gg 1 \text{ (reptation)} \quad (38)$$

In PMC theory the end-to-end vector correlation function and the shear modulus are not rigorously proportional to each other in general. Elsewhere,[30,31,34] it was

found that in the frequency window $1/\tau^{RR} \ll \omega \ll 1/(\tau_0 N_e^2)$ the following connections hold:

$$G'(\omega) \sim G_N \quad \text{and} \quad G''(\omega) \sim G_N \frac{M''(\omega)}{N} \tag{39}$$

$$\langle \mathbf{P}'(\omega)\cdot\mathbf{P}(0)\rangle \sim R_g^2 \quad \text{and}$$

$$\langle \mathbf{P}''(\omega)\cdot\mathbf{P}(0)\rangle \sim R_g^2 \frac{(\Sigma''(\omega))^{-1/2}}{N^{5/4}} \tag{40}$$

where the single/double primes denote storage/loss functions. The simplified diffusive center-of-mass relaxation of the entanglement constraints as described by the memory functions $\tilde{\Sigma}$ and $\tilde{M}$, eqs 36 and 37, leads to results identical to those from the reptation/tube model, i.e., eq 38. In the frequency window $1/\tau^{RR} \ll \omega \ll 1/\tau^{R}$, considering the reptative-like coherent decay channel only, then eqs 34, 36, 37, 39, and 40 immediately lead to eq 38. These reptation-like results in intermediate frequency windows have to be contrasted with the correct PMC results[30,31,34] that, in the specified frequency window and using the frozen matrix approximation, follow from eqs 15, 27, 33, 39, and 40:

$$G''(\omega) \sim G_N(\omega\tau_0 N^{9/2})^{-1/4} \tag{41}$$

$$\langle \mathbf{P}''(\omega)\cdot\mathbf{P}(0)\rangle \sim R_g^2(\omega\tau_0 N^{23/6})^{-3/8} \tag{42}$$

Without derivation let us recall the results for higher frequencies but still below the crossover frequency to the Rouse behavior:[30,31,34] $G''(\omega) \sim G_N(\omega\tau_0 N^{16/3})^{-3/16}$ and $\langle \mathbf{P}''(\omega)\cdot\mathbf{P}(0)\rangle \sim R_g^2(\omega\tau_0 N^{40/9})^{-9/32}$.

Reptation and PMC theory therefore describe similar friction contributions acting on the tracer polymer. The asymptotic N-scaling of the transport coefficients agrees, but a different mode spectrum or intermediate time dependence arises from the treatment of the internal shape fluctuations in the PMC approach. Neglecting the shape fluctuations, PMC theory recovers the reptation results, as both theories then assume that entanglements only relax via the coherent center-of-mass diffusion of the tracer polymer. Tracer shape fluctuations in the PMC equations do not lead to changes in the asymptotic, Markovian results for the conformational dynamics but do affect the initial decay in the final disentanglement process. It is just in this intermediate frequency window where the exponents and the overall shapes of the shear moduli predicted by PMC theory are in much better agreement with experimental measurements than the reptation/tube predictions.[31,34,50−52] Note that shallow slopes, $G''(\omega) \sim \omega^{-0.23}$, are found in the shear moduli of various polymeric systems,[50−52] whereas in dielectric loss[20,53−55] often somewhat higher exponents are measured, $\epsilon''(\omega) \sim \omega^{-0.21}$ to $\sim\omega^{-0.33}$.

The extensions of the tube model including contour fluctuations lead to shallower slopes in $G''(\omega)$ than pure reptation and also model the anomalous molecular weight dependence of the shear viscosity.[18,19] However, in our opinion these approaches do not accurately reproduce the observed power law N and ω scalings. Moreover, recent dielectric tracer experiments of Adachi and co-workers[20,21] find on the one hand a reptation-like scaling of the final relaxation time, $\tau_D \sim M^3$, for large polymer tracers in entangled polymeric matrices, but in the identical systems a shallow loss spectrum, $\epsilon''(\omega) \sim \omega^{-0.21}$ to $\sim \omega^{-0.31}$. They conclude this disproves the idea that the anomalous exponents in the viscosity versus molecular weight scaling and in the dielectric loss spectrum are connected. Such a conclusion is in good agreement with PMC theory, where two very different physical effects are the source of these behaviors. As discussed later in this section, within PMC theory tracer shape fluctuations lead to anomalous frequency power laws for the initial stages of the disentanglement process, and, finite size effects of the matrix constraints lead to nonasymptotic scaling of the transport coefficients.

B. Matrix Constraint Porosity and Constraint Release. Contributions to the memory functions $\Sigma(t)$ and $M(t)$, eqs 15 and 27, are characterized by spatially varying or wavevector dependent amplitudes and characteristic times. Within the PMC description one may view the static contributions or amplitudes in the mode coupling vertices as the strengths of the entanglement constraints on a length scale $2\pi/k$ on the tracer dynamics. The time dependence described by the normalized propagators captures the disentanglement processes. The net friction is obtained from the summation of friction amplitudes on all length scales weighted by the characteristic rates required for decay of the corresponding constraints.[6] Let us first recall the previous results where the matrix was assumed to be dynamically frozen in the PMC model.[6,31,34] This corresponds to setting $S_k(t) = S_k$ in eq 15. The relaxation of the entanglement friction then only proceeds via the probe collective dynamics calculated in the RR model. In the asymptotic limit of a large degree of polymerization of the tracer, the intrinsic (N-independent) characteristic length scales like b, ξ_ρ, and σ become widely separated from $R_g \propto \sqrt{N} \to \infty$. Thus, eq 15 further simplifies as the wavevector dependence of the matrix structure factor, S_k, and the direct correlation function, c_k, can be neglected. Also, the asymptotic result of eqs 34 and 35 can be used, and the PRISM Ornstein−Zernicke equation, $S_k = \omega_k + \rho_m h_k$ together with eq 13 leads to the replacement[28] $S_0\rho_m c_0 \approx -1$. The suppression of the center-of-mass diffusion coefficient, $\hat{\Sigma}_0$ in eq 16, then is of the form:[29,31,34]

$$\hat{\Sigma}_0 \propto (g_d\sqrt{N})^2 \tag{43}$$

The entanglement friction is proportional to the square of the number of binary segmental contacts of a pair of interpenetrating polymer chains weighted by a factor proportional to the probability of contact, i.e., the intermolecular pair correlation function at the excluded volume distance. In PMC theory the fluctuating forces describing the entanglement friction therefore arise from excluded volume interactions of strongly interacting polymer chains. Their strength is given by the number of two macromolecule pair contacts, approximately N^2/R_g^3, and the contact site−site radial distribution function, g_d. The terminal relaxation time and viscosity follow as $\tau_D \propto \eta \propto R_g^2/D \propto g_d^2 N^3$.

It is well-known from neutron or light scattering experiments that the collective density fluctuations of a polymeric melt rapidly decay into equilibrium.[56−58] At least within the accuracy of the mentioned experiments, $S_k(t)$ has decayed to zero at times much shorter than τ_D. Naively, this contradicts the frozen matrix assumption in eq 15, which requires that $S_k(t)$ is nonzero on time scales where the tracer dynamics determines the decay of the entanglement friction.[5] However, obviously

it is not necessary that the full amplitude of the collective density fluctuations is frozen in. Strongly molecular weight dependent contributions to the tracer dynamics are already obtained if some small, but finite, N-independent amplitude of the matrix dynamics only relaxes at times of the order of the probe dynamics as given by eq 33. Indeed, this is the experimental situation for the stress relaxation function $G(t)$, where $G_N \ll \rho_m k_B T$. Little is known experimentally and theoretically about the existence, magnitude, and time dependence of an entanglement plateau in $S_k(t)$ in the melt.[56−58] In Θ solutions, however, the plateau in $S_k(t)$ has been observed and there the general expectation has been verified that its amplitude is proportional to the ratio of shear to compressibility modulus.[59] Note that for nearly incompressible melts the sensitivity of neutron or light scattering is not sufficient for direct observation of such small amplitudes.

The question of the entanglement amplitude in the slow matrix dynamics motivated the rederivation of the PMC equations projecting onto the collective stress variables in section 2.A. Experimentally, the entanglement plateau in the stress modulus is well studied.[1] In this section it will be shown that straightforward assumptions lead to identical PMC expressions starting from either the choice of matrix density or matrix stress fluctuations as a slow collective variable and that the previous frozen matrix assumption nicely connects to established concepts.

Let us first comment on our treatment of binary polymer−solvent solutions, which we crudely model as an effective one-component polymer fluid. Adding a small molecule liquid to a polymeric liquid has two kinds of effects. First, the equilibrium structure of the polymeric subsystem is changed. The polymer density fluctuations grow, and the osmotic compressibility strongly increases.[2,3,23,45,46] Locally, the contact probability of segments on different macromolecules, i.e., g_d, goes down.[45,46] Also, the intramolecular structure can be changed depending on the type of solvent.[2,23,46] We will use a simple Gaussian chain model and an integral equation approach, PRISM,[44−46] in order to capture these effects as well as possible and study their consequences on the dynamics of entangled polymers.[32−34] A second group of effects of adding a solvent directly influences the dynamics of the polymer component. The local mobility, i.e., ζ_0, is strongly affected.[1] The two-component liquid mixture exhibits further transport processes, interdiffusion[35] or possibly gel-like modes,[60,61] which may couple to the polymer density fluctuations. Hydrodynamic interactions arise from the instantaneous but long-ranged solvent motions.[2,3,62] The local mobility affects our overall time scale and is taken from comparison with experiments. The remaining two effects described above are neglected. The standard argument is that the interdiffusion is fast following the solvent motion and that hydrodynamic interactions are screened.[3] Our approach therefore focuses on the effects of the liquid equilibrium structure on the dynamics but does not modify the basic dynamical equations with varying solvent content and quality.

The long-lived matrix constraints can be written as a wavevector dependent amplitude and a normalized time and (in general) wavevector dependent function:

$$S_k(t) = S_k f_k^S \Phi_k(t) \quad \text{where} \quad \Phi_k(t \ll \tau_D) = 1 \qquad (44)$$

The normalized correlation function, $\Phi_k(t)$, describes the final decay of the matrix constraints that possess the frozen-in amplitudes $S_k f_k^S$. Faster decay processes, the so-called microscopic and glassy relaxation processes, are assumed to be completed. They result in a decay of $S_k(t)$ from its initial value $S_k(t = 0) = S_k$ down to the arrested amplitude, $S_k f_k^S$ where $f_k^S < 1$. The importance of an amplitude of the final relaxation step smaller than unity has most clearly been recognized in the mode coupling theory of the glass transition.[42] There equations for the frozen in amplitudes f_k^S are derived. In the present context we will describe a physically plausible model and quote neutron scattering measurements in order to obtain a simple model for f_k^S.

The amplitude of the matrix constraints contains two spatially varying or wavevector dependent factors that describe what might be called the "porosity" of the entanglement constraints. First, the equilibrium matrix structure, S_k, describes a nonuniform compressibility of the surrounding polymeric liquid. We assume a simple Ornstein−Zernicke form that is appropriate for concentrated or (semi-) dilute Θ solutions and for wavelengths large compared to monomeric length scales.[2,3,45,46]

$$S_k = \frac{S_0}{1 + k^2 \xi_\rho^{\,2}} \qquad (45)$$

where ξ_ρ is the density screening length or "mesh-size", and $S_0 = \rho_m k_B T \kappa_T$, where κ_T is the isothermal (osmotic) compressibility of the polymer subsystem. The mesh size can be measured by neutron or other scattering techniques.[2] Alternatively, liquid state theories predict its magnitude and density dependence in agreement with blob scaling and field theoretical considerations.[32,45,46] In PRISM theory, the form of eq 45 and the additional result $c_k \approx c_0$ has been derived.[63,64] Whereas a melt is described by a density screening length of the magnitude of monomeric length scales, a less concentrated polymeric liquid exhibits a much larger ξ_ρ. ξ_ρ grows with decreasing concentration until, in the dilute solution limit, it agrees with the radius of gyration of a single polymer chain.[2] In good solvents, the correct form of the density susceptibility nontrivially deviates from the Ornstein−Zernicke form[2] of eq 45. As we require S_k in order to perform wavevector integrals only, we neglect these quantitative corrections. In this picture the difference between a good and a Θ solvent is only captured in the different dependence of monomeric length scales on the actual polymeric density. Whereas in a Θ solvent the statistical segment length scales are density independent, in a good solvent the excluded volume interaction leads to an effective monomeric size dependent on density,[2,32] $\sigma \sim \rho_m^{-1/8}$.

In eq 44, only an amplitude $f_k^S < 1$ of the total density fluctuations is arrested up to the disentanglement time τ_D. We follow Semenov[65] and Genz[66] in estimating the magnitude of its spatially homogeneous part, f_0^S, as the ratio of the shear modulus to the bulk modulus, or in our notation $f_0^S = S_0/N_e$. Note that in typical melts where $S_0 \approx 0.25$ and $N_e = 50-300$ one finds f_0^S is of the order of 10^{-2} or smaller. We shall not repeat the arguments of Semenov and Genz but rather derive the same result for $\Sigma(t)$ looking at the shear stress variables below. Clearly, the very local density correlations should not be arrested by the entanglement

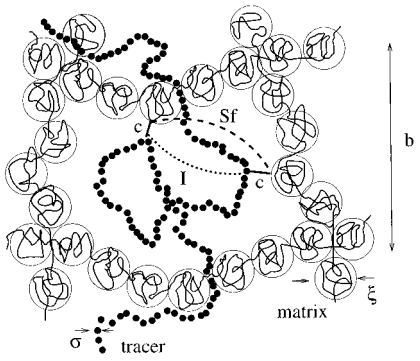

Figure 3. Schematic representation of the (static) entanglement constraints in the friction functions of the PMC theory. The tracer interacts via the short-ranged pseudopotential c (the direct correlation function) with the matrix polymers. The entanglement constraints of the matrix separate into local (density screening length ξ_ρ) compressibility (structure factor S) and mesoscopic (entanglement length b) elastic correlations (amplitude f). Note that only a small number of the matrix polymers are shown as the blobs of size ξ_ρ which fill space. The tracer exhibits different intramolecular correlations, I, for the uniform drag, $I^\Sigma \sim \omega$, and for the conformational friction, $I^M \sim \omega^2/k^2$. Note that the conformational friction coarse grains the matrix correlations over much larger spatial regions.

effect.[3,29] We follow the general conviction that there exists an entanglement length b, $b^2 = N_e\sigma^2$, that determines the spatial resolution of the matrix entanglement constraints. Adapting the results of Ronca,[67] de Gennes,[68] and des Cloiseaux[69] about the plateau in the collective single chain dynamic structure factor, f_k^ω, to the plateau in the collective matrix structure factor, f_k^S, we arrive at the following simple model:

$$f_k^S = (S_0/N_e)e^{-(kb/6)^2} \tag{46}$$

The entanglement length in the mentioned theoretical considerations and in the comparison with neutron scattering is defined by $f_{k=6/b}^\omega = e^{-1}$. We have checked explicitly that the simplified Gaussian shape assumption in eq 46 does not affect the results of our theory appreciably.

The sketch in Figure 3 of the matrix and tracer correlations and characteristic length scales summarizes the physical factors that enter the PMC memory functions. Clearly, in order to obtain the $N \to \infty$ asymptotic results, the tracer size, R_g, has to greatly exceed the matrix correlation lengths, ξ_ρ of the density fluctuations and b of the elastic mesh. It will be a central part of our results and their discussion that the intramolecular correlations of the tracer coarse grain over a much larger matrix volume in the conformational friction function, $M(t)$, than in the center-of-mass memory function, $\Sigma(t)$.

The form of the time dependence of the matrix constraints in $S_k(t)$ can be deduced by following the theoretical studies mentioned above.[65,66,68,69] The matrix provides entanglement constraints up to a time when the final disentanglement step of the matrix polymers takes place. The reptation/tube picture for the collective single chain correlator, and the PMC results for the generalized Rouse mode correlators,[6] indicate that this disentanglement process is characterized by a uniform, wavevector and Rouse mode independent relaxation time τ_D. The natural assumption for $\Phi_k(t)$, which also agrees with the theoretical finds of Semenov[65] and Genz,[66] therefore is[6]

$$\Phi_k(t) = \Phi(t) = e^{-(t/\tau_D)} \tag{47}$$

Using the eqs 44−47 in eq 15, and the original expression for the M-memory function[6,31,34] (containing $S_k(t)$), one obtains the final expressions of the PMC theory for the tracer diffusion coefficient, the disentanglement time τ_D, and the shear viscosity of linear chain polymers.[6,31] Since the disentanglement time τ_D is determined from the M-memory function, eq 30, but also enters in its relaxation, via eqs 27 and 47, a self-consistency aspect emerges. Before proceeding to its discussion and consequences for transport properties of the PMC theory, it is instructive to derive the same final equations based on the assumption that the collective stress variables are slow, i.e., starting from eq 27.

Equation 27 was obtained by assuming that the collective matrix stress variables are the slow variables hindering and slowing down the tracer dynamics. It is well-known that the final stress relaxation is characterized by the disentanglement time scale τ_D so that we can write[1−3] with eq 47:

$$G_k(t) = G_k f_k^G \Phi(t) \tag{48}$$

Neglecting small quantitative differences, the glassy elastic modulus can be approximated by

$$G_k \approx \rho_m k_B T(S_k/S_0) = \frac{\rho_m k_B T}{1 + k^2 \xi_\rho^{\,2}} \tag{49}$$

Equation 49 expresses the idea that the glassy, elastic stresses are of the order of k_BT per segment and their correlation length is the density screening length; note that this expression is only needed for inverse wavevectors large compared to the monomeric sizes. It is well established experimentally that the entanglement plateau in the shear modulus is a factor $1/N_e$ smaller than the glassy modulus.[1] We again follow the generally held idea that the entanglement length b determines the spatial correlations of the elastic constraints provided by the entanglements. A simple model for the wavevector dependent plateau in the shear modulus therefore is[67−69]

$$f_k^G = \frac{1}{N_e} e^{-(kb/6)^2} \tag{50}$$

It does not appear to be a coincidence that the original PMC equations considering the collective density fluctuations and the "new" PMC equations resulting from eqs 27 and 47−50, which consider the collective stress variables as slow, lead to identical expressions for the memory functions, $\Sigma(t)$ and $M(t)$, and consequently to the same theoretical results. Rather, we surmise that apart from small quantitative differences, identical expressions for the fluctuating force memory functions are obtained if the same physical assumptions are made. Namely, (1) the fluctuating intermolecular forces are projected onto the product of a tracer and a collective dynamical variable. (2) The resulting four-point correlation function is factorized as in eq 24, stating that the friction forces relax via the collective matrix dynamics and the collective tracer density fluctuations. (3) The collective tracer dynamic structure factor is evaluated within the RR model. (4) There is some long-lived, finite amplitude of the collective matrix constraints that only

relaxes during the final disentanglement process. Its spatial correlation length is b, the entanglement length. (5) The disentanglement time follows from self-consistently requiring the internal relaxation time to agree with the collective flow time.

Two important new ingredients result from the more detailed treatment of the matrix constraints as compared to the previous frozen matrix considerations. First, the constraint release mechanism, i.e., the consideration of the time dependence of the matrix constraints, relaxes the unphysical assumption that some collective degrees of freedom do not relax into equilibrium. Instead, the known slow dynamics of the disentanglement process enters the theory in a self-consistent way. Moreover, the variation of the tracer dynamics with matrix molecular weight can now be studied. Second, the treatment of the constraint porosity is improved. Whereas some previous numerical studies[30,31] included the spatial variation of the compressibility via $\xi_\rho \neq 0$, the frozen-in elastic mesh, characterized by the entanglement length b, enters as a new length into the PMC fluctuating force memory functions. An immediate consequence of $b \neq 0$ is the prediction of much larger finite size corrections since the inequality $b \gg \xi_\rho$ holds in general, and finite size corrections within the PMC theory only vanish for R_g large compared to all other length scales.[6,31]

Note that the entanglement degree of polymerization, N_e, can be estimated from the theory, i.e., from the crossover calculation of the RR model, eq 35. However, it can also be obtained experimentally from a rheological measurement, $G_N = \rho_m k_B T/N_e$. In the following we will use the prediction of the present version PMC theory that entanglement corrections enter as a function of N and N_e in a scaled fashion N/N_e; section 4.B discusses the reasons for this. Thus, we assume N_e to be known experimentally and express results in terms of N/N_e.

4. Asymptotic and General Finite Size Results

A. Asymptotic Predictions. The predictions of the PMC model in the asymptotic, $N \to \infty$, limit have been worked out previously.[6,31,33,34] We first recall these results for the transport coefficients.

Changes of the polymer transport coefficients depending on tracer molecular weight result from the long-ranged contributions ($k \propto R_g^{-1}$) of the entanglement friction. The matrix constraint amplitudes and their friction contributions in the Σ- and M-memory functions differ due to the different intramolecular weighting factors, $k^4\omega_k$ and $k^2\omega_k{}^2$ in $\Sigma(t)$ and $M(t)$, respectively. For Gaussian chain polymers a simple, but rather accurate, expression for the intramolecular structure factor is[3]

$$\omega_k = \frac{N}{1 + k^2 R_g{}^2/2} \tag{51}$$

Figure 4 shows the intramolecular factors of the entanglement amplitudes in the Σ- and M-memory functions. Global entanglement constraints, on the size of the tracer, dominate in the conformational memory function, $M(t)$, only. The diffusive tracer dynamics, eq 33, enhances the small wavevector contributions to the Markovian, transport coefficients. Figure 4 shows that, for conformational dynamics and stress relaxation, long wavelength ($kR_g \approx 1$) contributions extending across the size of the tracer molecule contribute most. In the center-of-mass friction $\Sigma(t)$ local modes dominate the amplitude associated with entanglement constraints,

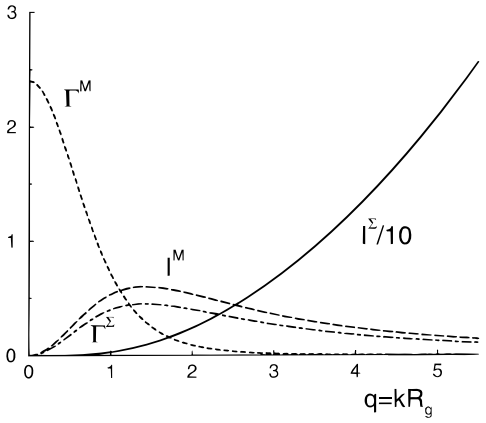

Figure 4. Intramolecular factors determining the entanglement constraint amplitudes in the conformational, I^M (long dashes), eq 63, and in the center-of-mass, I^Σ (solid line, scaled by 1/10), eq 62, friction functions plotted versus reduced wavevector, $q = kR_g$. The corresponding asymptotic friction amplitudes, $\Gamma^\Sigma = 2I^\Sigma\hat{\omega}/q^2$ (chain curve) and $\Gamma^M = 2I^M\hat{\omega}/q^2$ (short dashes), follow from the diffusive relaxation rates, $2\hat{\omega}_q/q^2$, of the RR model in eq 33.

although $kR_g \approx 1$ contributions dominate the long time (Markov) friction coefficient renormalization. In PMC theory, this difference in weighting of force correlations is the origin of the different, property-specific molecular weight scaling of the corrections to the Rouse, single polymer dynamics that is so characteristic of entangled polymeric systems.

The diffusion coefficient follows from the uniform drag memory function, $\Sigma(t)$ eqs 15 and 16 plus the new analysis of section 3.B:

$$D = D^R\left[1 + \lambda_D \frac{N}{N_e}\right]^{-1} \tag{52}$$

where the Rouse diffusion constant, $D^R = (k_B T/\zeta_0 N)$, is the result for a single macromolecule immersed in a continuum system characterized by an instantaneous friction coefficient,[3,24] ζ_0. A reptation-like asymptotic scaling is obtained as the corrections to the Rouse result are of quadratic order in the parameter[29,31,34] ($g_d\sqrt{N}$). The strength parameter of the PMC corrections relative to the Rouse result, i.e. λ_D, is proportional to a well-defined, and in principle independently measurable, quantity: the mean-squared, averaged intermolecular force exerted by the matrix polymers on the probe center-of-mass per unit density

$$\lambda_D = \frac{32}{3\alpha} \sim \langle |F|^2 \rangle/\rho_m \tag{53}$$

It is important to note that in general λ_D and α, which is defined in eq 53, are expected to be density and material dependent parameters. This result differs from the reptation prediction where $\lambda_D = 3$ is a universal number independent of solvent character, chemical structure, and density of the polymeric system.[3]

The inverse strength parameter α will play the most important role in quantifying the finite size corrections in the PMC approach and can be more explicitly written as[5,32]

$$\frac{1}{\alpha} = \frac{S_0}{2}(\rho_m g_d c_0 S_0)^2 \sim \langle |F|^2 \rangle/\rho_m \tag{54}$$

Note that in previous PMC work, e.g., ref 33 and earlier publications,[5,6,28−31,34] the literal frozen matrix ap-

proximation lead to an expression for α of the form: $1/\alpha \propto g_d^2 N_e$. As will be discussed in the following paper, no significant changes in previous results for the concentration dependence of polymeric transport coefficients arise from this difference on the basis of PRISM input for simple Gaussian chain models. The actual magnitudes, however, of the PMC dynamical parameters now come out in almost quantitative agreement (perhaps fortuitously) with experimental measurements. The parameter α also determines the prefactor of the asymptotic final disentanglement time, and by assumption, of the shear viscosity:

$$\eta = \eta^R\left(1 + \lambda_\eta\left(\frac{N}{N_e}\right)^2\right) \tag{55}$$

where the Rouse result, $\eta^R = \rho_m \zeta_0 \sigma^2 N/36$, again follows for a single Gaussian polymer in a continuum with friction coefficient ζ_0 but without hydrodynamic interactions.[3] Here λ_η is connected to α via:

$$\lambda_\eta = \frac{12}{\alpha} \tag{56}$$

which again can be compared to the reptation prediction[3] of $\lambda_\eta = 15/4$. These equations predict a universal ratio of the diffusion constant and shear viscosity in the asymptotic limit:

$$\frac{\eta D}{R_g^{\,2}} \to G_N \frac{\lambda_\eta}{6\lambda_D} = G_N \frac{3}{16} \quad \text{for} \quad N \to \infty \tag{57}$$

Remarkably, the value of the constant $\lambda_\eta/6\lambda_D = 3/16$ is very close to the reptation result of 5/24. Note, however, that the prefactors λ_D and λ_η are, in general, material and thermodynamic state dependent and that their close connection via the parameter α follows from two key points of the PMC theory. First, the treatment of the translation−rotation coupling discussed in context with eqs 11 and 26, and second, the assumption that the entanglement friction in the uniform and the conformational memory functions, $\Sigma(t)$ and $M(t)$, decays via the identical tracer dynamical process, i.e. the RR collective intramolecular density fluctuations. Of course, the neglect of hydrodynamic interactions and the simplified treatment of solutions possibly could also affect eq 57. The exact numerical factors in eqs 53 and 56 depend on the exact form of the intramolecular structure factor ω_k used in the vertices. The values denoted above result when, for analytical convenience, the simple approximation eq 51 with $R_g^2 = N\sigma^2/6$ is used.

The asymptotic result for the conformational relaxation time, τ_D, is directly connected with eq 55: $\tau_D/\tau_0 = N^3/(\alpha N_e)$. This result may also be taken as the (experimental) definition of the (inverse) entanglement strength parameter α. Note, that the reptation/tube result, $\tau_D = 3\tau^R(N/N_e)$, differs from this PMC result in the prediction of a universal value of the asymptotic prefactor, $\alpha = \pi^2/3$ for reptation, whereas α is given by eq 54 in PMC theory. Dielectric relaxation, which measures the end-to-end-vector correlation function, $\langle \mathbf{P}(t)\cdot\mathbf{P}(0)\rangle$, does not exactly determine τ_D, as it weights global modes much more heavily than viscoelastic measurements. From the spectrum of modes obtained in PMC theory after neglecting the tracer chain ends, as discussed in section 2.A and refs 6, 31, and 34, one can easily calculate an average dielectric relaxation time, $\tau^\epsilon = \int_0^\infty dt\, \langle \mathbf{P}(t)\cdot\mathbf{P}(0)\rangle/\langle \mathbf{P}(0)\cdot\mathbf{P}(0)\rangle$. In a dielectric spectrum, it describes the low-frequency behavior, $\epsilon''(\omega) \propto \omega\tau^\epsilon$ for $\omega\tau^\epsilon \ll 1$. We find

$$\tau^\epsilon/\tau^R = \frac{\pi^2}{12}[1 + \lambda_\epsilon n] \quad \text{where} \quad \lambda_\epsilon = 32/\alpha \tag{58}$$

The difference in the asymptotic limit, $\tau^\epsilon/\tau_D \to 32/12$, arises from the contributions of the low lying modes to the end-to-end-vector fluctuations, which are described by $\Sigma'(t)$ in eqs 1 and 26. Naturally, the approximation to neglect the chain end effects[34] when diagonalizing eq 1 will lead to the largest systematic errors for the low lying modes and therefore in quantities like τ^ϵ.

B. Parameters and Magnitudes of Finite Size Corrections. The asymptotic predictions for the transport coefficients of a tracer derived above assumed frozen-in constraints of the surrounding polymer matrix. A simple additivity approximation was used in order to describe the crossover from unentangled Rouse to entangled PMC dynamics. In the rest of this manuscript and the following paper, we will discuss corrections to these results arising from the spatial correlations and the time dependence of the matrix constraints or entanglements. The aim is not to describe more accurately the low molecular weight regime, $N \le 5N_e$, but to study the effects that prevail up to the highest molecular weights that are experimentally accessible. As will be discussed, finite N corrections are predicted, which vanish for $N \to \infty$ but, depending on the situation studied, are not yet negligible for $N/N_e \approx 10^3$. It is for such corrections at rather high $N/N_e > 5$ that we hope our simple models for the matrix constraints and the Rouse to entangled dynamics crossover to be appropriate. As well-defined equilibrium structural information is required, improvements can easily be considered if better (experimental) information is available. The deviations of the transport coefficients from the Rouse values depend on molecular weight via the ratios $n = N/N_e$ and $p = P/P_e$ only, where N (N_e) is the tracer and P (P_e) the matrix polymer degree of polymerization (entanglement degree of polymerization). The physical origin of this scaling is the existence of the entanglement length, b. Entanglements form an elastic mesh of spacing b and slow down the polymer dynamics only if the intramolecular correlations of the tracer extend over distances larger than b. The entanglement friction of a polymer of size R_g therefore depends on the ratio $R_g^2/b^2 \sim N/N_e$. This result, however, rests upon our corrected identification of the frozen-in amplitudes of the entanglement constraints, i.e., $f_0^S \sim S_0/N_e$ in eq 46 or $f_0^G \sim 1/N_e$ in eq 50.

The asymptotic results, eqs 52 and 55, are determined solely by the rescaled molecular weight, n, and the intermolecular excluded volume strength factor, $1/\alpha$. From the comparison with the reptation/tube predictions for the diffusion constant and viscosity, it appears that a value of $\alpha \approx 3$ should be considered reasonable[3] at least under melt conditions. In the following paper[22] we will give further arguments using PRISM results and comparisons with experiments for this choice. The finite size corrections depend on a second, dimensionless material dependent parameter, δ, where

$$\delta = \xi_\rho/b \tag{59}$$

δ is the ratio of the compressibility length scale (physical mesh), ξ_ρ, to the elastic mesh size, b. The appearance of this ratio again follows from the spatial origin of

entanglements within the PMC theory. The constraints arise due to equilibrium, eq 45, and dynamically frozen-in, eq 50, intermolecular correlations. Again, we generally expect δ is a material and density dependent parameter. As will be discussed in the following paper,[22] from the recent comprehensive neutron scattering and rheological study,[70] and theoretical PRISM and computer simulation results, values of ξ_ρ and b are known for a variety of polymers and varying density conditions. On the basis of this data, we estimate $\delta \approx 0.05$ for melts and somewhat larger values for solutions,[71] $\delta \leq 0.3$.

PMC theory differs from the reptation picture in that it generally predicts a material dependence in the asymptotic transport coefficients even when expressed in reduced variables. Moreover, the appearance of the structural correlations, parameterized by δ, has no analog in the tube description, which sets effectively $\delta = 0$. This statement does not concern the scaling considerations for the asymptotic transport coefficients nor plateau moduli[2,72,73] but addresses the finite size corrections, i.e., the speeding up of the dynamics, due to the correlations of the entanglement constraints.

Introducing the reduced variable, $q = kR_g$, the two memory functions of the PMC approach, $\Sigma(t)$ from eq 15, and $M(t)$ from eq 27, can be written using the two nonuniversal parameters α and δ:

$$\Sigma(t) = \frac{2\lambda_D}{\tau_0}\frac{\sqrt{n}}{N^2}\int_0^\infty dq\, I^\Sigma(q)\, \hat{S}(q\delta/\sqrt{n}) \times \hat{f}(q/\sqrt{n}) e^{-[q^2(t/\tau_D)/\Theta\hat{\omega}_q]} e^{-(t/\tau_D)} \quad (60)$$

$$M(t) = \frac{\lambda_\eta}{3\tau_0}\sqrt{n}\int_0^\infty dq\, I^M(q)\, \hat{S}(q\delta/\sqrt{n}) \times \hat{f}(q/\sqrt{n}) e^{-[q^2(t/\tau_D)/\Theta\hat{\omega}_q]} e^{-(t/\tau_D)} \quad (61)$$

where the reduced compressibility, $\hat{S} = S_k/S_0$, follows from eq 45 and the elastic frozen-in amplitude, $\hat{f}$ normalized to $\hat{f}(0) = 1$, from eq 50. The first time dependent factor in eqs 60 and 61 arises from the tracer, eq 33, the second from the matrix dynamics, eq 47. The amplitudes of the entanglement forces are proportional to the spatial weights:

$$I^\Sigma(q) = \frac{q^4\hat{\omega}_q}{\int dq'\, q'^2\hat{\omega}_{q'}{}^2} \quad (62)$$

$$I^M(q) = \frac{q^2\hat{\omega}_q{}^2}{\int dq'\, \hat{\omega}_{q'}{}^3} \quad (63)$$

where the rescaled intramolecular structure factor, $\hat{\omega}_q = \omega_{(k=q/R_g)}/N$, appears. An important quantity specifying the relevance of the constraint release mechanism compared to the tracer dynamics is the ratio, denoted as Θ, of the tracer RR time scale to the matrix disentanglement time:

$$\Theta(n,p,\alpha,\delta) = \frac{(\zeta_{tr}^{RR}/\zeta_0^{tr})N^2}{2(\tau_D^m/\tau_0^{tr})} = \frac{\tau_0^{tr}}{\tau_0^m}\frac{P_e}{N_e}\frac{\alpha}{2\beta(p,\alpha,\delta)}\left(\frac{n}{p}\right)^3\frac{\gamma(\delta/\sqrt{n})}{\sqrt{n}} \quad (64)$$

where $\gamma(\delta/\sqrt{n}) = \int dq\ q^2\hat{\omega}_q{}^2\hat{S}(q\delta/\sqrt{n})/\int dq\ q^2\hat{\omega}_q{}^2$ describes the finite size corrections in the RR Markovian calculation, eq 34; $\gamma(x) \to 1$ for $x \to 0$. Equation 64 indicates one source of variation if tracers of chemistry different from the matrix polymers are studied. The monomeric friction coefficients and the appropriate entanglement molecular weights will differ in general. However, also the vertex and consequently α, eq 54, will differ, as the total intermolecular site−site corelation function, h_k, eq 13, is changed by different tracer−matrix coupling depending on the chemical interactions.[45] Therefore, we restrict our considerations to chemically identical tracer and matrix polymers in the following (except for section 6); i.e., $(\tau_0^{tr}/\tau_0^m)(P_e/N_e) = 1$ in eq 64.

The factor $\beta(p,\alpha,\delta)$ in eq 64 describes the reduction of the disentanglement time relative to its asymptotic value:

$$\tau_D/\tau_0 = \frac{\beta(p,\alpha,\delta)}{\alpha}\frac{P^3}{P_e} \quad (65)$$

where $\beta \to 1$ for $p \to \infty$ follows from eqs 30 and 61. β is found as the solution of the self-consistency equation, requiring that the matrix disentanglement time agrees with the longest internal relaxation time of one of the matrix polymers.

$$\beta(p,\alpha,\delta) = \int_0^\infty dq\, I^M(q)\, \hat{S}(q\delta/\sqrt{p}) \times \hat{f}(q/\sqrt{p})\frac{\gamma(\delta/\sqrt{p})}{\Theta(p,p,\alpha,\delta) + q^2/\hat{\omega}_q} \quad (66)$$

If the matrix disentanglement time, τ_D, is found from eqs 64−66, the same equations determine the tracer internal relaxation time with the obvious replacements, especially $\Theta(p,p,\alpha,\delta) \to \Theta(n,p,\alpha,\delta)$ in eq 66 and $p \to n$ elsewhere.

The shear viscosity including the finite size corrections and the crossover to the unentangled Rouse result then follows as:

$$\eta = \eta^R[1 + \lambda_\eta p^2\beta(p,\alpha,\delta)] \quad (67)$$

Note that our crossover model qualitatively, but presumably not quantitatively, correctly describes the viscosity at low molecular weights. The longest relaxation time, τ_D, however, does not crossover to the Rouse time, $\tau^R = \tau_0(P/\pi)^2$, with decreasing P but goes to zero below a certain P. It is at such low molecular weights, $P \approx P_e$, where the self-consistency equation, eqs 64 and 66, loses its validity.

From the so-determined matrix disentanglement time, τ_D, the diffusion coefficient of a tracer can be calculated using eqs 16 and 60:

$$D = \frac{k_B T}{\zeta_0 N}[1 + \lambda_D n K(n,\delta,\Theta(n,p,\alpha,\delta))]^{-1} \quad (68)$$

where the reduction of the asymptotic entanglement friction constant follows from the Σ memory function, eq 60:

$$K(n,\delta,\Theta) = \int_0^\infty dq\, I^\Sigma(q)\, \hat{S}(q\delta/\sqrt{n}) \times \hat{f}(q/\sqrt{n})\frac{\gamma(\delta/\sqrt{n})}{\Theta(n,p,\alpha,\delta) + q^2/\hat{\omega}_q} \quad (69)$$

Again, the crossover to the Rouse result is described qualitatively, but possibly not quantitatively, correctly.

In order to compare with dielectric loss measurements of the end-to-end-vector fluctuations,[20] we must include the finite size corrections into eq 58 for the relaxation time, τ^{ϵ}, of the end-to-end-vector correlation function of a tracer in a polymer matrix. Two qualitatively different finite size corrections appear in τ^{ϵ} as the conformational memory function, $M(t)$, but also the homogeneous friction function, $\Sigma'(t)$, affect the low lying, global modes of an entangled polymer. It is shown in refs 6, 31, and 34 that the generalized Rouse mode correlators of PMC at zero frequency have the following form: $C''_p(\omega = 0)/C_p(t = 0) = \tau_0[(N/\pi p)^2(1 + \hat{\Sigma}'_0) + \hat{M}_0]$. One notices the mode independent relaxation rate, $\tau_0\hat{M}_0$, which dominates the viscoelastic dynamics, and the Rouse-like rates, which show the familiar $1/p^2$ mode dependence and are negligible except for the lowest modes. From this, summing over the odd modes,[3] $p = 1, 3, ...$, of the end-to-end-vector correlation function at zero frequency, one obtains the dielectric relaxation time, τ^{ϵ}:

$$\tau^{\epsilon} = \tau_0\frac{N^2}{12}\Big[1 + (24\beta(n,p,\alpha) + 8K'(n,p,\alpha,\delta))\frac{n}{\alpha}\Big] \quad (70)$$

where K' is the normalized finite size correction arising from the time integral over the uniform friction function, $\Sigma'(t)$:

$$K'(n,p,\alpha,\delta) = \int_0^{\infty} \mathrm{d}q\, I^{\Sigma'}(q)\, \hat{S}(q\delta/\sqrt{n}) \times \hat{f}(q/\sqrt{n})\frac{\gamma(\delta/\sqrt{n})}{\Theta(n,p,\alpha,\delta) + q^2/\hat{\omega}_q} \quad (71)$$

K' differs from $K(n,p,\alpha,\delta)$, eq 69, in the contributions from the intramolecular structure only:

$$I^{\Sigma'}(q) = \frac{q^6\hat{\omega}_q{}^2}{\int \mathrm{d}q'\, q'^4\hat{\omega}_{q'}{}^3} \quad (72)$$

The quantity β in eq 70 follows from eqs 64 and 66 with the replacements denoted there, and the numerical prefactors in eq 70 assure the correct limiting behavior, eq 58, as $\beta \to 1$ and $K' \to 1$ for $p \to \infty$. Again, we suggest eq 70 for intermediate and large molecular weights of the tracer, n, and of the matrix polymers, p. When comparing to experimental data, it has to be kept in mind that our present results apply for chemically identical tracer and matrix polymers only. System specific variations will arise from differences in the monomeric friction coefficients, in the molecular weights of entanglement (see eq 64) and from different local packings, i.e., g_d, and effective potentials, c_0, in eq 54.

It is one of the central results of the PMC theory that the entanglement effects on the center-of-mass motion and the conformational dynamics are closely connected via the two memory functions[6,31,34] $\Sigma(t)$ and $M(t)$. They differ in the intramolecular weighting factors, I^{Σ}_q/N^2 eq 60, and I^{M}_q eq 61, only. Note from Figure 4 that I^{M}_q, eq 63, is peaked around $q = kR_g \approx 1$, whereas I^{Σ}_q, eq 62, monotonically increases with increasing q. Friction contributions on the global, macromolecular size scale determine the internal relaxations. This is one of the central findings of PMC,[6] which also agrees with the reptation/tube idea that a motion of the whole chain is necessary in order to relax internal fluctuations.[2,3] This behavior of I^{M} strongly differs from the (tightly connected) finding that contributions to the friction of the center-of-mass motion, i.e., I^{Σ}, eq 62, arise from more local correlations.[31] See Figure 4 where the entanglement amplitudes and the friction contributions, i.e., the amplitudes weighted by the corresponding relaxation rates (in the asymptotic, frozen matrix limit), are shown.

This difference causes three major consequences of PMC theory. First, the asymptotic slowing down of the internal modes is larger by a factor N^2 than the extra friction exerted on the center-of-mass.[6] Second, the porosity or spatial correlations of the matrix constraints, $S_k < S_0$ and $f^S_k < f^S_0$, influence the center-of-mass motion more strongly. The uniform drag friction function, $\Sigma(t)$, is much more sensitive to the actual values of the finite, material dependent length scales, ξ_ρ and b. The conformational friction function, $M(t)$, on the other hand, is relatively independent of these nonuniversal parameters. Third, the entanglement friction can decay via the constraint release mechanism, i.e., the decay of the matrix constraints following eq 47, or via the tracer collective structural dynamics of the RR model, which exhibits a diffusive pole, eq 33. Comparing the two decay rates for different wavevectors, the tracer dynamics will dominate the decay at large wavevectors, $q = kR_g \gg 1$, and the matrix dynamics will dominate in the limit $q = kR_g \to 0$. Therefore, the constraint release mechanism will lead to much larger finite size corrections in the conformational friction function, $M(t)$, than in $\Sigma(t)$, as a much larger portion of the entanglement constraints arises for $q = kR_g < 1$ in M than in Σ. The internal dynamics and the viscosities, therefore, will be dominated by the constraint release mechanism in general, whereas the constraint porosity will mainly influence the center-of-mass motion. In the following sections we discuss these differences and other aspects of the finite size effects in more detail by numerically solving eqs 60−69 for the physically relevant parameter ranges, $\alpha \approx 3$ and $\delta = 0$−0.3.

5. Predictions for Transport Properties and Relaxation Times

A. Effects of Constraint Release on the Viscosity. Considering a melt of polymers with degree of polymerization $N = nN_e$, the nonlinear equation for the finite N suppression, $\beta(n,\alpha,\delta)$ eq 66, of the disentanglement time can be easily solved numerically. β depends on the molecular weight via the dimensionless ratio $n = N/N_e$ only. The nonuniversal parameters α, where $1/\alpha \sim \langle|F|^2\rangle/\rho_m$ in eq 54, and δ, eq 59, lead to, in general, density and chemical structure dependent results. Results for β are shown in Figure 5 spanning a wide range of possible variations in α and especially δ. Since in melts $b \approx 35$−90 Å depending on chemical structure,[70] it is apparent from Figure 5 that the density screening length has to be increased to unphysically large values, $\delta = \xi_\rho/b \approx 0.5$, in order to observe changes in β in the range $n \geq 5$, where our equations are reliable. From the discussion in section 4.B of which spatial correlations dominate the respective friction functions, it can easily be understood that the internal relaxation time τ_D is only affected by the constraint release mechanism but not by the constraint porosity. The disentanglement time, τ_D, and as a consequence the viscosity, η, follow from the conformational friction function, $M(t)$, which is most sensitive to constraints for $q = kR_g \approx 1$. These rather long range, intermolecular correlations decay more effectively via the matrix dynamics than via the diffusive RR tracer dynamics. The local spatial correlations of the entanglements, either the equilibrium correlation length, ξ_ρ, or the

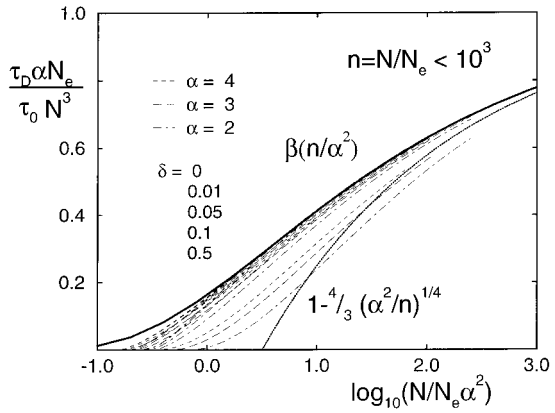

Figure 5. Finite size reduction factors, $\beta(n,\alpha,\delta) = \tau_D \alpha N_e/\tau_0 N^3$, of eq 65, for different entanglement strengths, $\langle|F^2|\rangle/\rho_m \sim 1/\alpha$, and length scale ratios, $\delta = \xi_\rho/b$. The thin lines correspond to the parameters α as denoted and to increasing parameter δ from left to right. The solid line shows the solution, $\beta(n/\alpha^2)$, neglecting constraint porosity, and the thin solid line shows the asymptote eq 73.

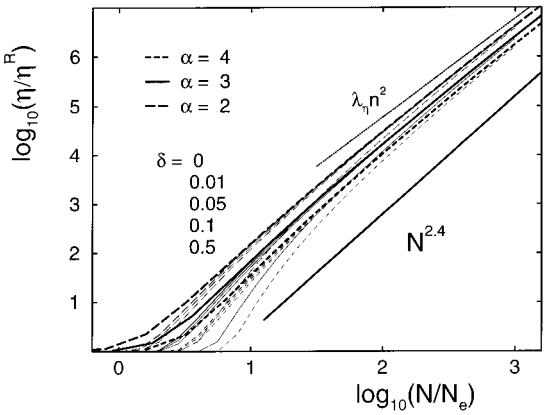

Figure 6. Ratios of shear viscosity to Rouse viscosity corresponding to the disentanglement times τ_D following from the results of Figure 5. Bold lines denote the results neglecting constraint porosity for different α, and the thin lines for fixed parameter α shift with increasing parameter δ from left to right. Lines of the same style belong to one value of parameter α. A power law, $\eta/\eta^R \sim N^{2.4}$, is shown for comparison. The $N \to \infty$ asymptote $\lambda_\eta(N/N_e)^2$ is drawn as a thin solid line for $\alpha = 2$ or $\lambda_\eta = 6$.

localization length of the frozen-in amplitude, b, influence the conformational dynamics only very weakly since the local contributions to $M(t)$ are virtually negligible.

Note that for physically reasonable choices[70,71] of δ, i.e., for $\delta \le 0.3$, almost no effects on β or τ_D can be seen in Figure 5 for $n \ge 5$. For $n \le 5$ smaller molecular weights our crossover model cannot be considered very reliable. Thus, we conclude that for experimentally relevant parameter ranges the disentanglement time, τ_D, or viscosity, η, is suppressed below its asymptotic value by the constraint release mechanism. To a good approximation the self-consistency equations, eqs 64 and 66, can therefore be simplified by neglecting the constraint porosity, i.e., setting $\hat{S}_q = 1$ and $\hat{f}_q = 1$ in eq 66. The correction factor β then depends on the ratio n^2/α only, i.e., $\beta(n,\alpha) = \beta(n/\alpha^2)$. Its asymptotic behavior can be found easily:

$$\beta(n/\alpha^2) \to 1 - \frac{4}{3}\left(\frac{\alpha^2}{n}\right)^{1/4} \qquad \text{for} \qquad n \to \infty \qquad (73)$$

The solid line in Figure 5 indicates the solution, $\beta(n/\alpha^2)$, to the self-consistency equations neglecting constraint porosity. The asymptotic behavior, eq 73, and the independence of δ for large n can be observed when comparing the solutions $\beta(n,\alpha,\delta)$, of eqs 64 and 66 including constraint porosity. A handy interpolation approximation to $\beta(n/\alpha^2)$ in the relevant molecular weight range is given by the following formula: $\beta(n/\alpha^2) = \exp\{-[x + 0.22x^2 + 0.01x^3 + 0.02x^4]\}$ where $x = 4/3(\alpha^2/n)^{1/4}$; in Figure 5 it lies on top of the exact curve, $\beta(n/\alpha^2)$. In the following, i.e., after Figure 6 in this paper and in the following paper, we will simplify the numerical work and neglect the constraint porosity corrections in the conformational dynamics. The above simple but accurate expression for $\beta(n/\alpha^2)$ will be used. Errors are thereby made in regions only where the simple matrix and crossover models we employ are not reliable anyway.

Figure 6 shows the predicted viscosities corresponding to these disentanglement times where the thick lines are given by the simplified expression neglecting the spatial constraint correlations:

$$\eta = \eta^R[1 + \lambda_\eta n^2 \beta(n/\alpha^2)] \qquad (74)$$

Again, in Figure 6 it is seen that only unrealistically large values of δ lead to appreciable deviations of η from the constraint release result, eq 74. Also, even though eq 74 does not lead to a rigorous power law behavior except in the asymptotic limit, $\eta \sim N^3$ for $N \to \infty$, an effective power law over 2 orders of magnitude with an exponent of $\approx$3.4 can be accurately fitted to the results. Note that the extremely slow approach to the reptation-like asymptote, $\eta \sim N^3(1 - c/n^{1/4})$, where $c = (4/3)\sqrt{\alpha}$, leads to considerable deviations even for $n \approx 10^3$, molecular weights which are difficult to achieve experimentally.[74] In Figure 5, for values $n = 10^3$, the correction factor, β, is still of the order 0.7 or less. Experimentally, of course, the very slow drift of β in that range may not be discernible in the data and an apparent power law with an exponent approaching 3 may be concluded for $n \ge 10^2 - 10^3$. Note that the apparent power law $\eta \sim N^{3.4}$ holds in a molecular weight range $n \ge 10$, where our crossover model and the considerations about the matrix structural functions may be oversimplified but are qualitatively correct and contain all the physics expected to arise in full numerical PMC calculations. As our prediction is not a rigorous power law in the intermediate n range, it is difficult to estimate what effective exponents could be reported when fitting power laws to eq 74. The results will also depend on the window in molecular weight of the fits. Exponents up to 3.5 seem easily achievable.

Two effects of the inverse strength parameter α on the viscosity can be seen arising from the constraint release mechanism. First, asymptotically, the viscosity becomes proportional to $1/\alpha$. Obviously, the stronger the intermolecular excluded volume forces are, the higher the viscosities will be in the entangled regime. Second, increasing α leads to more curvature and higher effective exponents in η as the PMC corrections to the Rouse result effectively set in at larger n only but then increase more rapidly with n. Finally, since our predicted finite N-corrections to the viscosity are essentially independent of $\delta = \xi_\rho/b$, we predict a sort of universality of the *non*asymptotic behavior nearly independent of both chemical structure and polymer concentration when η is expressed in terms of N/N_e. This prediction appears to be in excellent agreement with experiments, which find that the η versus N/N_e experimental power

laws are essentially identical in melts and solutions.[1,75] For the values of $n = 10-1000$ relevant to experiments, we find that Θ is typically in the range $\approx 1-0.1$. Thus we conclude that there is no wide separation between the characteristic single chain conformational relaxation time and the time scale for entanglement force decay. Hence, a non-Markovian situation is suggested under experimentally accessible conditions.

Let us comment on another, non-Markovian consequence of the constraint release mechanism, which will affect the PMC results for the frequency dependence of the shear modulus at rather low frequencies, $\omega\tau_D < 1$. When the matrix dynamics, i.e., the constraint release relaxation, eq 47, is neglected and when $\Phi(t) = 1$ in eq 61, the conformational friction function exhibits a long time tail,[29,31,34] $M(t \gg \tau^{RR}) \rightarrow \sqrt{N}(\tau^{RR}/t)^{3/2}$, where $\tau^{RR} = \tau_0 N^2\sqrt{n}$. This slow decay leads (for finite N) to an anomalous, low-frequency behavior in the storage part of $M(\omega)$, $M'(\omega) \sim \sqrt{N}(\omega\tau^{RR})^{3/2}$, which is more weakly dependent on frequency than the $M' \sim \omega^2$ expected from a Markovian separation of time scales. In numerical solutions to the full PMC equations,[76] neglecting the constraint release, it has been observed that this anomalous decay of the conformational friction function leads to a final disentanglement peak in $G''(\omega)$, which is quantitatively broadened for $\omega\tau_D < 1$ compared to the experimental data.[50−52] Obviously, the exponential matrix constraint relaxation, eq 47, yields $M(t) \propto e^{-(t/\tau_D)}$ (see eq 61), which will cut off the long time tail in M at the disentanglement time, τ_D. Therefore, we expect the quantitative discrepancy[76] between PMC results and experiments for shear moduli at low frequencies, $\omega\tau_D < 1$, will be resolved in future numerical solutions of PMC theory including the constraint release mechanism. Note that it also can be expected that no changes will be found for the high-frequency power law tails of the disentanglement process, $\omega\tau_D \gg 1$, where the analytic PMC prediction[29,31,34] of an $\omega^{-\Delta}$ law with $\Delta \approx 0.2-0.25$ and the numerical PMC results[31,76] agree nicely with shear measurements[50−52] but differ strongly with the pure reptation model prediction of $\omega^{-1/2}$.

B. Constraint Porosity Effect on Diffusion Constants for $P \gg N$. When a tracer polymer with degree of polymerization $N = nN_e$ is immersed into a polymeric matrix of degree of polymerization $P = pN_e$, the constraint release mechanism can be neglected if $p \gg n$. Then the matrix polymers are immobile relative to the tracer. In eq 64, the ratio of the corresponding time scales, Θ, vanishes, as is evident from the factor $(n/p)^3$. The entanglement friction in the memory functions then can relax only via the tracer collective structure factor (computed with the RR model). The resulting tracer diffusion coefficients will, in general, still show finite n corrections, as the matrix constraints are not homogeneously correlated, i.e., b/R_g and ξ_ρ/R_g are nonzero. The tracer center-of-mass experiences the full entanglement constraints only if it has to distort the frozen-in elastic mesh appreciably ($R_g \gg b$), and to compress the equilibrium structure uniformly ($R_g \gg \xi_\rho$). As the constraint amplitude contributions to the conformational dynamics arise from $q = kR_g \approx 1$, the internal conformational degrees of freedom are rather insensitive to the spatial finite size correlations. Therefore, in the limit $P \gg N \gg N_e$, the PMC approach predicts the reptation-like scaling, $\tau_D/\tau_0 = N^3/(\alpha N_e)$, for the internal relaxation time of a tracer polymer. The center-of-mass motion, however, because the more local intermolecular correlations contribute heavily, eq 62, does not feel the full entanglement constraints as long as the finite length scales, ξ_ρ, b are not negligible relative to R_g. The diffusion constants therefore are increased relative to the $N \rightarrow \infty$ asymptotic behavior. Moreover, even at a fixed scaled degree of polymerization N/N_e corresponding to R_g^2/b^2, we find that the density screening length, although small, leads to a nonuniversal reduction of the friction. Note that the screening length, ξ_ρ (at least in semidilute solutions), and the entanglement length, b, are much larger than monomeric sizes, i.e., σ or a persistence length for flexible polymers. Therefore, parametrization of the dynamical consequences of these length scales with a few chemistry dependent parameters, as done in our models eqs 45 and 46, seems justified.

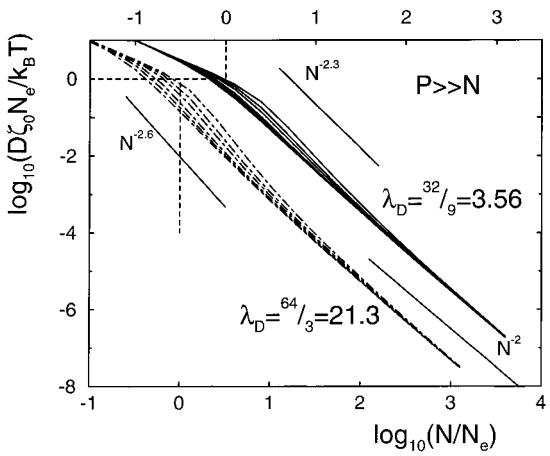

Figure 7. Tracer diffusion constants in the limit of immobile matrix polymers, $P \gg N$. Two sets of curves are shown with two different values of the asymptotic prefactor, λ_D, and correspond to the upper or lower horizontal scale. The curves show increasing steepness in the intermediate region with increasing $\delta = \xi_\rho/b$; $\delta = 0.01$, 0.05, 0.1, 0.2, 0.3, and 0.5, respectively. Three power laws with arbitrary prefactors are shown for comparison.

Figure 7 shows the tracer diffusion constants, D_∞^{tr}, for two values of the mean square force per density parameter, eq 54, $\alpha = 3$ and $\alpha = 1/2$, corresponding to $\lambda_D = 32/9$ and $\lambda_D = 64/3$, respectively. Values of the screening to entanglement length ratio, $\delta = \xi_\rho/b$, are chosen in a wide range. In the first case of $\lambda_D \approx 3.6$, which we suggest to be a melt-like case, a very rapid crossover from the Rouse, $D \sim 1/N$, to the asymptotic PMC result, $D \sim 1/(\lambda_D N^2)$ from eq 52, is seen for realistic melt values of $\delta \leq 0.05$, Importantly, in the range $n \geq 5$ almost no deviation from the asymptote can be observed. When δ is increased beyond its physically expected melt range, somewhat larger exponents in an effective power law, reaching up to $D \sim N^{-2.3}$ may be observed in the intermediate n-regime. In the second case, $\lambda_D \approx 21$, which we consider relevant for solutions (see the following paper), where also $\delta \leq 0.3$ is expected, an intermediate behavior appears in the range $1 \leq n \leq 50$. There the diffusion constant lies appreciably above its asymptote. For example, for $\lambda_D = 64/3$ and $\delta = 0.3$ ($\delta = 0.05$) at $n = 5$ the diffusivity is increased by a factor $D\lambda_D n/D^R \approx 3.7$ (1.8), respectively. In this n-range, a free fit to the numerical results would also lead to N-scaling exponents exceeding the classical reptation result appreciably. In Figure 7 a power $D \sim N^{-2.6}$ is drawn for comparison. The crossover to the true asymptote happens at much larger molecular weights in the solution case than in the melt case.

Note that these deviations from the reptation-like scaling have no analog within the extended reptation/

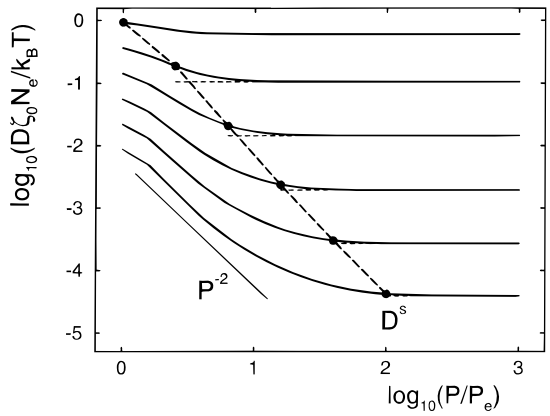

Figure 8. Tracer diffusion coefficients in a polymer melt as a function of matrix molecular weight, P/P_e, for different tracer degrees of polymerization, N/N_e; $\log_{10}(N/N_e) = 0$, 0.4, 0.8, 1.2, 1.6, and 2 from top to bottom. The parameters employed, $\alpha = 3$, $\delta = 0.05$, and $\lambda_D = 3$, are argued to describe a polymer melt. The self-diffusion constants, D^s, are denoted by circles and long dashes and can be compared to the asymptotic, D^{tr} for $P \to \infty$, values shown with horizontal short dashes. A power $D \sim P^{-2}$ is shown for comparison.

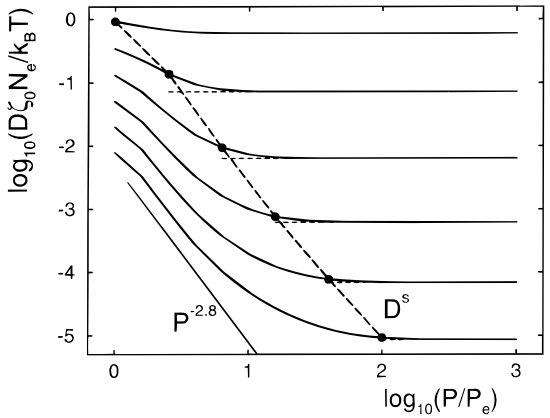

Figure 9. Tracer diffusion coefficients in a polymer solution as a function of matrix molecular weight, P/P_e, for different tracer degrees of polymerization, N/N_e; $\log_{10}(N/N_e) = 0$, 0.4, 0.8, 1.2, 1.6, and 2 from top to bottom. The parameters employed, $\alpha = 3$, $\delta = 0.3$, and $\lambda_D = 18$, are argued to describe a polymer solution or a melt exhibiting a special tracer-matrix polymer interaction. The self-diffusion constants, D^s (circles and long dashes), the asymptotic values, D^{tr} for $P \to \infty$ (short dashes), and a power $D \sim P^{-2.8}$, are shown.

tube ideas. Constraint release is irrelevant because of the arrested matrix dynamics, $P \to \infty$, and the contour length fluctuation mechanism of Doi[18,19] does not affect the N-scaling of the tracer diffusion constants. It appears that a microscopic approach incorporating the liquid structure properly is required to identify these finite size corrections arising from the spatial correlations of the matrix entanglement constraints. Chemistry and density or composition dependence is expected for these effects. Also note that in contrast with the reptation prediction, the asymptotic prefactor for the PMC, λ_D, is nonuniversal and is expected to be polymer-density dependent.

C. Variation of Tracer Diffusivities with Matrix Molecular Weight. The variation of the tracer diffusion constant upon changing the matrix molecular weight can also be described within our general approach. Because of the neglect of the matrix dynamics in the RR calculation, the theory is restricted to the range $p = P/P_e > 1$. First, the matrix disentanglement time has to be found from the self-consistency equation, eqs 64 and 66. Then the suppression of the entanglement effects on the center-of-mass motion of the tracer can be calculated from eqs 68 and 69. Figure 8 shows the case with parameters argued to be relevant for polymer melts. With increasing P a rather rapid crossover of the tracer diffusion constant from its Rouse value, D^R, to the strongly entangled value, D_∞^{tr}, discussed in section 3.D, is observed. The self-diffusion coefficients, D^S for $N = P$, are also indicated and generally fall in the transition region between the two asymptotes, D^R and D_∞^{tr}. In Figure 8, the parameters $\alpha = 3$, $\delta = 0.05$, and $\lambda_D = 3$, lead to a little overshooting of the asymptotic D_∞^{tr} relative to the N^{-2} asymptotes.

The dependence on matrix molecular weight in the crossover region is not a rigorous power law but, if approximated by one, corresponds to exponents of the order of 2. This exponent is smaller than the limiting ideal behavior of $D \sim P^{-3}$ expected from Graessley's constraint release formulation[15] and $D \sim P^{-2.5}$ expected from Klein's analysis.[16,17] However, if different material parameters are chosen, in Figure 9 we use $\alpha = 3$, $\delta = 0.3$, and $\lambda_D = 18$ corresponding to dense solutions, then larger effective exponents are found. Clearly, the dependence on the matrix molecular weight must be weaker than the one following from $D^{tr} \sim 1/\tau_D(P)$, as this result would hold only if the tracer dynamics was totally frozen in and solely the constraint release mechanism, or matrix dynamics eq 47, would relax the entanglement constraints in $\Sigma(t)$, eq 60. In this solution-like case, a stronger matrix molecular weight dependence in the transition range is observed compared to the melt case. $D \sim P^{-2.8}$ is drawn for comparison in Figure 9. Again, the self-diffusion coefficients lie in the crossover region. For the case of Figure 9, the constraint porosity is also important and leads to deviations of D^{tr} from the asymptotic predictions for all matrix molecular weights, as discussed in section 5.B. Note that the values of the diffusivities in the solution case lie below the corresponding (same $n = N/N_e$) melt diffusion constants because of the larger prefactor, λ_D, of the large N asymptote.

In Figure 9 (and slightly also in Figure 8), for the sake of discussion, the theoretically predicted correlation of λ_D with α, eq 53, was violated. In this case, α determines the matrix disentanglement time τ_D and the viscosity via the eqs 61 and 64−67 but not the strength factor, λ_D, in the Σ-memory function, eq 60, describing the tracer. If the matrix viscosities corresponding to Figures 8 and 9 were plotted, they would agree, but the tracer internal relaxation time would differ from the matrix one. An experimentally relevant situation where such a breaking of the relation in eq 53 can appear is in the case of a tracer that differs chemically from the matrix polymers. Then the intermolecular correlation function, h_k in eq 13, which determines the vertices or constraint amplitudes, is expected to be different. That is, intermolecular tracer−matrix packing is not the same as the pure matrix−matrix correlations. Specific tracer−matrix−polymer chemical interactions caused by the addition of selective solvent could also lead to such a more complicated situation.

D. Variation of Tracer Dielectric Times with Matrix Molecular Weight. The dynamics of a tracer polymer in a polymeric matrix is slowed down by the entanglement constraints. In the limit of rapidly moving matrix polymers, the Rouse model with instantaneous friction coefficient, ζ_0, would apply for the tracer. Dielectric spectroscopy[20,21] measures the slowing down

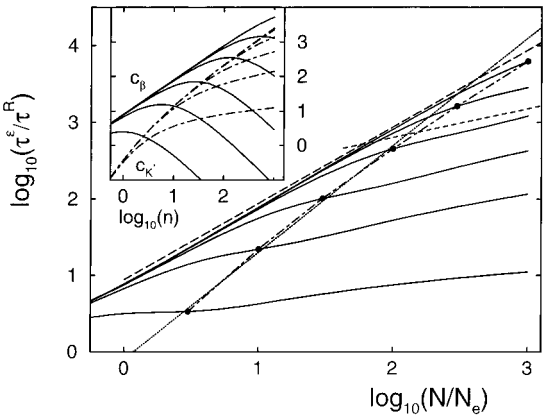

Figure 10. Tracer dielectric relaxation time, τ^ϵ, normalized by the Rouse time as a function of reduced tracer molecular weight, $n = N/N_e$, for different matrix molecular weights, $p = P/P_e$: $p = 3$, 10, 30, 100, 300, and 1000 from bottom to top. Melt-like parameters, $\alpha = 3$ and $\delta = 0.05$, are chosen. Chemically identical tracer and matrix polymers are considered. The asymptotes, $\tau^\epsilon \sim N^3$ for $n \ll p$ (long dashes) and $\tau^\epsilon \sim N^{19/8}$ for $n \gg p$ (short dashes), are included. The matrix end-to-end-vector relaxation times, shown with circles and a dashed-dotted line, correspond to $n = p$. A thin solid line shows a power law, $\tau^\epsilon \sim N^{3.4}$, fitted through these $n = p$ system points. The inset separately shows the logarithm of the contributions in eq 70 from the conformational friction corrections, $c_\beta = 24\beta n/\alpha$ (solid lines), and from the homogeneous friction, $c_{K'} = 8K'n/\alpha$ (chain curves).

of the relaxation time of the end-to-end-vector correlation function, τ^ϵ of eq 70. Asymptotically, the scaling, $\tau^\epsilon \sim N^3$, eq 58, is predicted by PMC theory.

As the global modes contribute to τ^ϵ appreciably, in general, τ^ϵ differs from the internal, conformational disentanglement time τ_D. Whenever it is justified to neglect the contributions from the uniform drag friction, i.e., $c_{K'} = 8K'n/\alpha \ll c_\beta = 24\beta n/\alpha$ in eq 70, then the relation $\tau^\epsilon = 2\tau_D$ holds. In this case, the conformational friction determines the dielectric relaxation time, τ^ϵ, and therefore, results independent of the spatial constraint correlations, constraint porosity, but strongly dependent on the constraint release mechanism are predicted by PMC theory. Whenever the uniform friction arising from $\Sigma'(t)$, eq 26, dominates the dielectric relaxation time, strong constraint porosity effects resulting from the finite lengths scales, $b/R_g > 0$ and $\xi_\rho/R_g > 0$, are predicted in the PMC approach. Note that the neglect of chain end effects, discussed in section 2.A, strongly affects the global mode contributions in eq 70. Without exact numerical diagonalizations of the full equations of motion, eq 1, no estimate of the resulting errors in τ^ϵ can be given. As Figure 10 shows, this uncertainty mainly affects the results for τ^ϵ in the limit of large tracers in entangled matrices, $n \gg p \gg 1$. Melt-like parameters, $\alpha = 3$ and $\delta = 0.05$, are used for Figure 10.

Our model, eq 70, rests upon the assumption of strictly identical matrix and tracer polymers, which may differ in degree of polymerization only. Due to the approximations in the RR model, the results apply for entangled polymeric matrices, $p = P/P_e > 1$ only. Also, the curves are physically relevant for $\tau_D/\tau^R \approx c_\beta \gg 1$ only, where the connection between the conformational friction function and the final time scale, eq 30, holds. Note that τ_D from eq 65 does not, as would be required physically, cross over to the Rouse time in the limit $N \gg P$ but vanishes asymptotically because of $c_\beta \sim p^3/n^{3/2}$ for $n \gg p$. This limitation is not a fundamental one, but rather a consequence of our simplified modeling of the Rouse to entangled crossover.

In Figure 10 one notices that, apart from small quantitative corrections, the conformational friction determines the dielectric relaxation time, τ^ϵ, for tracers in strongly entangled matrices, i.e., for $n \le p$. For various matrix molecular weights, the dielectric, τ^ϵ, and internal, τ_D, relaxation time follow the asymptotic, $\tau/\tau^R \sim n$, behavior for $n \ll p$. For $n > p$, the uniform friction contributions to τ^ϵ dominate as they increase asymptotically, $c_{K'} \sim p^{3/4}n^{3/8}$ for $n \gg p \gg 1$. For long tracers in shorter, but still entangled, matrix polymers, PMC theory therefore predicts an intermediate power law behavior, $\tau^\epsilon \sim N^{19/8}$ for $n \gg p \gg 1$, resulting from the contributions of the global modes to the dielectric spectrum. The matrix dielectric relaxation times agree with the τ^ϵ of a tracer of identical degree of polymerization, $n = p$, and show a $\tau_D \sim N^{3.4}$ behavior for large n, as is also observed in the viscosity for this choice of strength parameter, $\alpha = 3$.

The constraint release mechanism and the constraint porosity thus strongly affect the molecular weight scaling of the dielectric relaxation time τ^ϵ. Note, however, that the high-frequency wing of the disentanglement process, as described by PMC theory, is connected to the tracer shape fluctuations. The physical origin of the fractal frequency behavior, e.g., $\langle \mathbf{P}''(\omega)\cdot\mathbf{P}(0)\rangle \sim \omega^{-3/8}$, eq 42, or $\langle \mathbf{P}''(\omega)\cdot\mathbf{P}(0)\rangle \sim \omega^{-9/32}$ for higher frequencies, therefore is predicted to be very different from the one determining the τ^ϵ scaling with N. In the limit $P \gg N$, where reptation-like scaling in the time scale $\tau \sim N^3$ is found since the matrix constraints cannot decay appreciably, the shape fluctuations of the tracer still speed up the early stages of the disentanglement process and lead to a much reduced high-frequency slope for $P''(\omega)$ at intermediate frequencies, $\omega\tau_D \gg 1$; see the discussion in section 3.A.

6. Extension of PMC Theory to Polymer Transport through Random, Gel-like Media

The diffusion of polymer tracers through amorphous media is of considerable interest in both physical and biological science.[77−79] On the one hand, the original reptation theory was formulated for the situation of a polymer in a gel.[4] On the other hand, gel electrophoresis constitutes a powerful but still poorly understood technique to characterize polymers, mostly biological ones.[79] In the present section we cannot address the multitude of different realizations of amorphous materials or of finite driving fields in electrophoresis. However, the unique aspect of PMC theory is that it connects the dynamics of polymers to the underlying structure of the surrounding matrix. This allows one to study a number of interesting tracer−gel cases within the same formalism. Moreover, the structural information, i.e., the spatially resolved compressibility and the mesh of elastic constraints, that uniquely determine the transport properties of a polymer tracer (if its intramolecular correlations are specified), raises the possibility of predicting the tracer dynamics from purely static experimental data.

In PMC theory an amorphous solid or gel is characterized by the time independence of the matrix constraints the probe feels. That is, in eq 44 or 48, $\Phi(t) = 1$. Cross-linked polymeric gels or silica gels exhibit arrested density structures that do not relax into homogeneous, liquid-like equilibrium. The constraint release mechanism therefore is not operative.

In order to describe gels that are fractal and exhibit pores on all (relevant) length scales, a simple fractal

ansatz for the density correlations is used:

$$S_k = \frac{S_0}{(1 + k^2\xi_g{}^2)^{D_F/2}} \tag{75}$$

where ξ_g is a characteristic mesh or pore size. Operationally, the gel fractal dimension is defined by a scattering experiment in the intermediate, self-similar spatial range, $k\xi_g \gg 1$, where $S_k \sim k^{-D_F}$ is seen. Exponents in the range $D_F \approx {}^5/_3-2$ apply to polymeric gels prepared by cross-linking (good) polymer solutions.[2]

Note that eq 75 describes a very simple model of a gel and in reality may not be adequate for experimental systems. Effects like quenched disorder of cross-links[80] are not described by eq 75 but can be put into S_k if the appropriate experimental or theoretical information is available. It should be mentioned that quenched cross-linking disorder introduces heterogenieties[80] on an even larger length scale than ξ_g, which results in enhanced values of S_k at small k. For example, the following form has been shown to fit experimental data on some gels[80]

$$S_k = \frac{S_0}{1 + k^2\xi_g{}^2} + S_{xc}e^{-(k\xi_{xc})^{0.7}}$$

where $\xi_{xc} > \xi_g$. In the spirit of our approach, which does not differentiate between quenched and annealed disorder, such a structure in S_k would lead to further nonuniversal finite size effects in the polymer tracer dynamics extending to even higher tracer molecular weights, as found in the present study.

The density screening length, ξ_g, can be considered to be the size of the largest pores in the gel. It separates the homogeneous density structure from the self-similar intermediate range. Of course, the breakdown of eq 75 at microscopic length scales is neglected for the dynamics of entangled polymers.

Two distinct classes of gels can be defined following the discussion of the constraint porosity in section 3.2. First, in a structurally rigid or "hard" gel, the mass density structure can be thought to pose strong constraints on the motion of a probe. The full amplitude of the gel density fluctuations therefore is expected to contribute to the entanglement friction functions. This formally corresponds to

$$f_k^S = 1 \tag{76}$$

in eq 44. Silica gels presumably belong to this class of hard gels.[81] A second class includes "soft" gels prepared from cross-linked polymer solutions. Even though the entanglement constraints then are permanent due to the cross-linking reaction, it cannot be expected that the strength of the so-formed elastic mesh significantly exceeds the strength of the non-cross-linked, time-dependent precursor. The model of section 3.2 should therefore apply and the constraint amplitudes again contain a small factor:

$$f_k^S = (S_0/N_e)e^{-(kb/6)^2} \tag{77}$$

For lack of detailed knowledge about the spatial correlations of the elastic mesh in cross-linked gels, we continue using a Gaussian ansatz for the wavevector dependence of f_k^S. Different k-dependent functions will affect the comparison with experiments only in so far as shifts in the poorly a priori known (fit) parameters occur.

In the soft gel models, the ratio ξ_g/b for cross-linked polymer gels is expected to be of the order of the values found for non-cross-linked polymer solutions[2] ($\delta = \xi_\rho/b \approx 0.3$). Larger values are expected in the so-called strangulation regime, where the high cross-linking density forces the entanglement length to become smaller than the one caused by the temporary cross-links.[11]

The question of the intramolecular structure of a polymer in a fractal medium is very complex and still not well understood.[78] Ideal, Gaussian-like intramolecular correlations cannot be expected in general. The mass-size scaling exponent, ν, where $R_g \sim N^\nu$, may even depend on the degree of polymerization, $\nu = \nu(N)$, and on other system-specific features.[78] We will neglect these difficulties and assume a fractal model with fixed mass-size exponent, ν, for the tracer polymer as well:

$$\omega_k = \frac{N}{(1 + ck^2R_g{}^2)^{(1/2\nu)}} \tag{78}$$

where $c = [(1 + 2\nu)(1 + \nu)/d]/(2\Gamma(1 + 1/2\nu))^{2\nu}$. From the obvious generalization of the Σ-memory function, eq 15, one obtains the following results for the tracer diffusion coefficient in a fractal gel in d-space dimensions:

$$D^{tr} = \frac{k_BT}{\zeta_0 N}[1 + \lambda_g N^{4-2d\nu} K_g(R_g/\xi_g, \xi_g/b)]^{-1} \tag{79}$$

where

$$K_g(R_g/\xi_g, \xi_g/b) = \frac{\int dq\, q^{d-1}\hat{\omega}_q{}^2\hat{S}(q\xi_g/R_g)\,\hat{f}^S(qb/R_g)\int dq\, q^{d-1}\hat{\omega}_q{}^2\hat{S}(q\xi_g/R_g)}{(\int dq\, q^{d-1}\hat{\omega}_q{}^2)^2} \tag{80}$$

The dynamics is predicted to depend strongly on the ratio R_g/ξ_g. This dependence of the tracer diffusion coefficient on the ratio of the tracer size relative to a mesoscopic length scale that characterizes the matrix mesh, is closely connected to the constraint porosity effects discussed in section 5.2. The latter have been shown to be important in polymer solutions or if special tracer−matrix chemical interactions exist.

The strength parameter λ_g in eq 79 can, in principle, be determined from the tracer−gel structural correlations, i.e., the pair contact value and the direct correlation function, c_k. For example, the PRISM description of binary polymeric liquids can be evaluated in the limit of vanishing tracer concentration.[45,46] However, because of the possibly varying chemical interactions of the tracer with the gel pore walls, no general statement about the magnitude of λ_g is possible. Moreover, the increase in the amplitude f_k^S, eq 77, which likely results from the cross-linking, also increases λ_g but cannot be described theoretically at present. Note that in the true polymer solution case, i.e., chemically identical tracer and matrix polymers, eq 77 applies, $\nu = 1/D_F = 1/2$, and λ_g is connected to λ_D, eq 53, via $\lambda_g = \lambda_D/N_e$. For more rigid gels, however, larger strength parameters, λ_g, are expected. Moreover, all λ's are proportional to the tracer−gel interaction strengths and therefore are expected to increase if the tracer polymers

adsorb to the gel pore walls, or if other specific tracer−gel or tracer−solvent interactions exist. Values much larger than λ_D/N_e therefore are possible for λ_g.

From eq 79 the asymptotic scaling of the tracer diffusion coefficients with molecular weight can be inferred, as the finite size correction factor, K, eq 80, approaches unity for larger tracers, $R_g \gg \xi_g$. Asymptotically, $D \sim N^{-5+2d\nu}$ is found independent of the gel fractal dimension.[29,34] In 3-dimensions, for ideal coil tracers, the classic $D \sim N^{-2}$ law is recovered. Note that eq 79, in the same way as our melt and solution descriptions, includes a crossover model describing the tracer diffusion constant for all tracer molecular weights; for the unhindered tracer the Rouse model is again chosen to apply. The PMC results including finite size effects therefore present a unified description of the tracer dynamics in gels arising from the competition of free and entangled polymer motion, where the second contribution depends on the length scale ratio R_g/ξ_g. In this respect the PMC theory differs from phenomenological approaches like the entropic barrier model of Muthukumar and Baumgärtner,[78,82−84] where special geometric considerations for $R_g \approx \xi_g$ are invoked, and the asymptotic limits ($R_g \gg \xi_g$ or $R_g \ll \xi_g$) and smooth regime crossovers are not included in the description.

Figure 11 shows tracer diffusion coefficients resulting from eqs 79 and 80 for fractal dimensions corresponding to self-avoiding random walk polymers, $\nu = 1/D_F = 3/5$ in the Flory approximation.[2,23] Gel pore sizes, ξ_g, are denoted by stating the degree of polymerization of a tracer whose radius of gyration agrees with ξ_g, i.e., $\xi_g = R_g(N)$. Results for two different values of λ_g are shown in order to explore the variation with this unknown system-specific parameter.

In Figure 11 one notices that deviations from the Rouse, unconstrained diffusion start for R_g/ξ_g below 1 but do not lead into the asymptote, $K_g(x \to \infty, y) \to 1$, up to very high degrees of polymerization of the tracer. Intermediate effective power law behavior arises with varying exponents, $D \sim N^{-2.3}$ to $D \sim N^{-2.7}$, depending on the parameters varied in Figure 11. The steepest molecular weight dependences fall into a range where the tracer R_g exceeds the gel pore size ξ_g appreciably. This finding appears to disagree with the entropic trapping ideas,[78,82−84] where maximal nonasymptotic results are centered around $R_g \approx \xi_g$. In the case of PMC theory the finite size effects lead to anomalous exponents for much larger tracer sizes.

The results of eqs 79 and 80 very weakly depend on the fractal dimension of the gel. Assuming for simplicity the identical constraint strengths, i.e., λ_g in eq 79, the soft gel, eq 77, and the hard gel, eq 76, lead to similar intermediate effective power laws. Somewhat higher exponents result for soft gels. Increases in the strength parameter, λ_g, lead to steeper crossover curves. Note that the existence of the entanglement length in the flexible mesh systems or soft gels leads to extended Rouse-like behavior, as the tracer has to uniformly distort the elastic mesh and, therefore, has to be larger, in order to feel the full entanglement constraints.

The degree of polymerization dependence of the diffusion coefficients, for intermediate tracer sizes, cannot be rigorously described by power laws. If, however, power laws are fitted to the numerical results, effective exponents clearly exceeding the reptation value of 2 are obtained. Note that this holds although the true asymptotic molecular weight dependence, $D \sim N^{-7/5}$ in Figure 11, is even *weaker* than the reptation-like

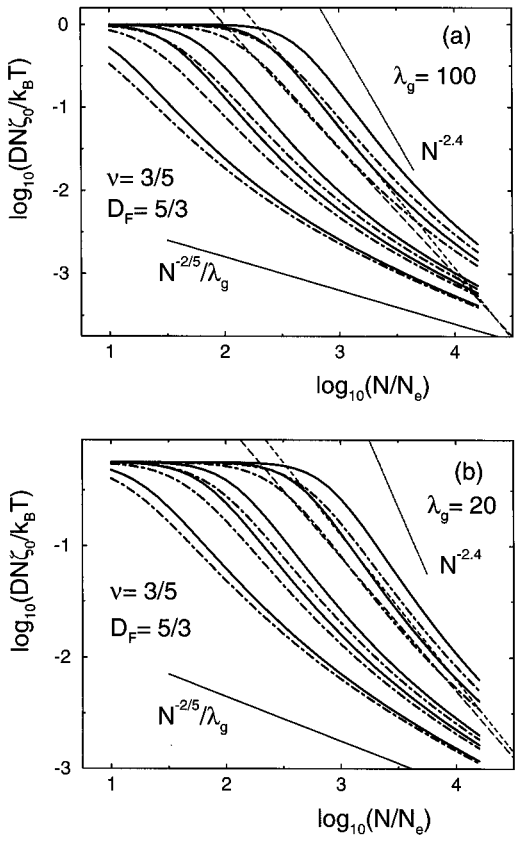

Figure 11. Tracer diffusion constants normalized by the Rouse result versus tracer molecular weight for tracer motion through gels with different pore sizes; the correlation lengths ξ_g agree with the radii of gyration of tracers of the degrees of polymerization, $N/N_e = 10$, 50, 100, 500, 1000. Tracer mass scaling exponent for a self-avoiding walk polymer, $\nu = 3/5$, and gel fractal dimension, $D_F = 5/3$, are used while fixing the interaction strength to $\lambda_g = 100$ in part (a) and $\lambda_g = 20$ in (b). For a soft, polymeric gel, eq 77, the ratio of screening and entanglement lengths is fixed to $\xi/b = 0.3$, and thick solid lines are drawn. Chain curves correspond to the hard, structurally rigid gel case, eq 76. The thin line is the asymptote $DN \to N^{-(4-2\nu d)}$, which meets the curves for $N/N_e \approx 10^8$. The maximal intermediate slope, $DN \sim N^{-(4-2\nu(d-D_F))}$, is shown as a thin solid line. In part (a), power laws, $DN \sim N^{-1.7}$ (short dashes) and $DN \sim N^{-1.5}$ (long dashes), are compared to the soft and hard gel calculations at $\xi_g = R_g(N = 500N_e)$, respectively. In part (b), power laws, $DN \sim N^{-1.3}$ (short dashes) and $DN \sim N^{-1.2}$ (long dashes), are compared to the soft and hard gel calculations at $\xi_g = R_g(N = 500N_e)$, respectively.

scaling. An upper bound to the effective exponents can be deduced from the small tracer size limit in eq 80. For $R_g/\xi_g \to 0$ one easily finds $K_g \sim (R_g/\xi_g)^{2D_F} \sim N^{2\nu D_F}$, which in the limit of a large asymptotic prefactor, λ_g, and/or large pore sizes leads to the upper bound, $D \sim N^{-5+2\nu(d-D_F)}$ where d is the spatial dimension. In the case of Figure 11 this estimate is $D \sim N^{-3.4}$.

7. Discussion

The predictions of PMC theory for the transport properties of entangled polymer melts, solutions, and gels are determined by the intramolecular and intermolecular equilibrium structural correlations. A number of approximations are necessary in order to simplify the N-generalized Langevin equations of eq 1.

1. The fluctuating intermolecular forces are approximated by their statistical overlap with the collective tracer structure factor and a collective matrix correlator in accord with known mode-coupling ideas. It is expected that, for any choice of slow matrix

variables, qualitatively identical PMC expressions result, as shown for the examples of matrix density and stress fluctuations.

2. The slow dynamics of the intermolecular forces is connected to the diffusive dynamics of the tracer and the (generally nondiffusive) disentanglement process of the surrounding matrix polymers.

3. The (projected) tracer dynamics entering the PMC friction functions is taken from a short time and/or small molecular weight calculation, the RR model.

4. The matrix or constraint release dynamics is evaluated from a self-consistency argument, requiring that the single polymer and matrix disentanglement time agree.

5. Simple models for the strength of the entanglement constraints exerted by the polymer matrix are formulated. They lead to qualitatively identical results when considering various slow matrix variables, as shown for the examples of density and stress fluctuations.

6. In order to calculate bulk transport properties or response functions for polymeric liquids, it is assumed that the entanglement effects arise from incoherently added, single chain contributions. For example, the bulk viscosities and dielectric susceptibility are derived from a single chain calculation.

7. Solutions are treated in the same way as melts, neglecting special dynamical effects, like "gel-modes",[60,61] but concentrating on the equilibrium structural changes.

Assumptions 6 and 7 are familiar from the reptation/tube theory and are generally motivated by the peculiarity of the entanglement effects to macromolecules (point 6), and the similarity of these phenomena in melts and solutions (point 7).

The robustness of the PMC results with regard to the identification of the slow matrix variables constraining the tracer polymer (points 1 and 5) rather reassuringly verifies that the structural correlations of the matrix constraints are characterized by two length scales, the entanglement length, b, and the density screening length, ξ_ρ. Whereas the first length scale is postulated and identified as the tube diameter in the phenomenological reptation approach, the effects of the second length scale on the dynamics are neglected there. In PMC theory, the matrix constraints are not fully developed if the ratio $\delta = \xi_\rho/b$ is not small. Smaller effective entanglement friction and finite size corrections then arise and vanish for large molecular weights only. The concept of "lack of full topological correlation of entanglement constraints" due to Muthukumar and Baumgärtner[78] bears some resemblance to our ideas, but there are significant differences.

The idea to equate the single chain and collective disentanglement times (point 4) appears rather natural and is also suggested by point 6. In a crude sense it is related to the constraint release mechanisms of Graessley[15] and Klein[16,17] within the phenomenological tube model framework, although there are strong differences. For example, these tube-based approaches are not self-consistent, and significantly affect only tracer diffusion and not conformational relaxation or viscosity in the $N = P$ case.

Employing the RR collective dynamical structure factor (point 3) in the PMC friction functions is suggested by the breakdown of the Rouse model for degrees of polymerization above N_e. Actually, N_e is defined by calculating where the Rouse model as a zeroth-order approximation is overwhelmed by the first-order correction, the RR model.[32] For the molecular weights and times required in the PMC friction functions, i.e., for $N \gg N_e$ and $t \gg \tau^R(N_e)$, the RR correlator is physically more reasonable than the Rouse correlator. Nevertheless, this aspect of the theory seems the most "uncontrolled". The use of a fully self-consistent correlator, i.e., entering the PMC correlator into the friction functions of PMC theory, is not appropriate, if naively implemented, since it results in a severe overestimation of the entanglement friction and an arrest ("macromolecular scale localization transition") at a finite degree of polymerization.[29,31]

The determination of the decay of the intermolecular forces from the collective dynamic structure factor of the tracer bears close connection to one of the central assumptions of reptation: the coherent center-of-mass motion of the chain in the tube determines the conformational relaxation.[2,3] In agreement with this picture, PMC theory finds, when tracer shape fluctuations are neglected, identical results for the conformational dynamics as for reptation. Not only the N-scaling of the internal relaxation time and viscosity agree but also the shear stress spectrum shows the high-frequency asymptote, $G''(\omega\tau_D \gg 1) \sim \omega^{-1/2}$, familiar from the tube survival function of reptation.[2,3] In better agreement with measurements of shear and dielectric spectra, PMC results[28,31,34] including tracer shape fluctuations find more shallow slopes, $G''(\omega\tau_D \gg 1) \sim \omega^{-x}$, where $x \approx 0.2-0.25$. In agreement with recent dielectric measurements of Adachi and co-workers,[20,21] these nonreptation-like power law behaviors are predicted to persist even if, for strongly entangled polymer matrices, the asymptotic scaling of the internal relaxation time, $\tau_D \sim N^3$, is observed.

Whereas the tracer shape fluctuations only influence the initial decay of the disentanglement process, there arise two finite size effects in PMC theory that affect the transport coefficients of entangled polymers. Both are closely connected as they arise from the consistent model for the matrix entanglements discussed in section 3.B. First, a decrease of the entanglement friction results from the time-dependent decay of the matrix constraints, termed the constraint release mechanism. Clearly, this idea bears similarity to Graessley's[15] or Klein's[16,17] ideas for tracer diffusion (but not viscosity), although the actual implementations strongly differ. PMC theory describes the decrease of the effective friction coefficient whereas in refs 15−17 two independent relaxation rates (or diffusion constants) are added on the basis of the assumed statistical independence of the reptation and constraint release transport processes. Second, the spatial correlations of the matrix constraints, termed constraint porosity, enhance the tracer motion as the full constraints are effective only if the intermolecular forces are summed over finite spatial regions. The constraint correlations are of two distinct origins: spatial compressibility, characterized by the density screening length or mesh size, ξ_ρ, and elastic mesh or entanglement length, b, correlations.

One of the central findings of the PMC approach is the result that entanglement constraint contributions to the conformational dynamics arise from globally, across the tracer, correlated intermolecular forces, whereas the center-of-mass friction results from more local intermolecular forces.[6] The corresponding constraint amplitudes are either peaked around $kR_g = 1$ or increase monotonically; see Figure 4. Perhaps this finding is connected to the reptation idea that the

mobility of the polymer in the tube can be motivated by the picture of "pulling a wet rope through a tube".[2] The motion of the whole "rope" is slowed down by short-ranged friction, whereas conformational relaxation requires the decay of the tube correlations due to the motion of the chain ends.[2,3] Also, the aspect of an underlying diffusive collective tracer dynamics, i.e., the collective RR dynamical structural factor, agrees with this picture.

A first consequence of the difference in the spatial correlations of the conformational, $M(t)$, and the uniform, $\Sigma(t)$, memory functions is their very different Markovian values,[6] $\hat{M}_0 \sim N^3$ and $\hat{\Sigma}_0 \sim N$. Because of this feature of strongly different effects of the entanglements on the internal and the center-of-mass friction, the prediction of conformational and stress relaxation arrest (plateau) but continued (but slowed down anomalous) segmental diffusion follows.

A second consequence, worked out in this paper, is the very different sensitivity to finite size effects predicted by PMC theory for internal and center-of-mass dynamics. Again, because of the rather long-ranged spatial correlations of the entanglement friction in the conformational dynamics, constraint porosity is irrelevant there. However, the constraint release mechanism strongly speeds up the conformational dynamics as it overwhelms the slow tracer RR dynamics on long length scales or for small wavevectors. The center-of-mass motion, on the other hand, is accelerated due to the decrease of the entanglement friction on local, finite length scales. The constraint porosity, therefore, enhances the diffusion constants of tracer polymers even in matrices of effectively immobile matrix polymers.

Two nonuniversal, microscopically defined parameters, the inverse entanglement strength parameter, α, and the length scale ratio, $\delta = \xi_\rho/b$, are predicted to control the finite size corrections to the ratios of the transport coefficients relative to their Rouse values if molecular weights are normalized by the corresponding entanglement molecular weight. The first parameter exists in the reptation/tube approach, where a universal value, $\alpha \approx 3-4$, is calculated. The second parameter has no analog there.

PMC theory predicts an extremely slow approach of the disentanglement time, τ_D, and hence the viscosity to their asymptotic, $\eta \sim \tau_D \sim N^3$, behavior. Higher exponents result from fits of effective power laws to the numerical PMC results for molecular weights $n = M/M_e < 10^3$. No clear separation of the final disentanglement time from the time scale for entanglement force decay is expected in experimentally relevant parameter ranges.

Diffusion constants for polymer tracers in matrices of immobile polymers are unaffected by the constraint release process but differ from the asymptotic behavior, $D \sim N^{-2}$, because of the spatial variation of the entanglement constraint amplitudes. Figure 7 exemplifies that for the experimentally relevant intermediate molecular weights effective exponents, $D \sim N^{-x}$, with x significantly exceeding the classical value of 2 will often occur.

The variation of the tracer diffusion constants upon varying the molecular weight of the matrix polymers results from a combination of both types of finite size effects. Strong variations are obtained due to the constraint release mechanism for systems where the matrix polymer molecular weight is smaller or slightly larger than the tracer molecular weight.

Constraint release and porosity also compete in the finite size corrections of the end-to-end-vector relaxation time, τ^ϵ, measured in dielectric spectroscopy.[20,21] In the limit of immobile matrix polymers, the disentanglement and dielectric times are proportional and follow the asymptotic scaling, $\tau_D \sim \tau^\epsilon \sim N^3$. In the limit of large tracer polymers in entangled matrices, a new behavior of τ^ϵ is predicted, $\tau^\epsilon \sim N^{19/8}$. It results from the global mode contributions in the dielectric spectrum and requires $M \gg P \gg M_e$, where M, P, and M_e are the tracer, matrix polymer, and entanglement molecular weight, respectively.

The dynamics of tracer polymers in amorphous solids, especially in gels, does not require qualitatively new physical effects to be appended to the PMC description once the physically appropriate generalizations of the matrix and tracer structure are made. Obviously, in an amorphous solid the entanglement constraints cannot fully relax, and hence the constraint release mechanism is absent. The constraint porosity, however, leads to strongly molecular weight dependent tracer diffusivities, especially as the tracer−gel interactions may often lead to stronger intermolecular forces than in simple homopolymer systems. For non-Gaussian intramolecular correlations of the tracer polymer, $R_g \sim N^\nu$, PMC theory does not predict reptation like results, but rather $D \sim N^{-5+2d\nu}$ asymptotically in d spatial dimensions. Very much stronger intermediate molecular weight dependences are predicted, however, arising from the constant porosity corrections as long as the ratio of gel pore size, ξ_g, to tracer size, R_g, is not negligible. In the limit of large tracer−gel interactions an upper bound, $D \sim N^{-5+2\nu(d-D_F)}$, may be approached, where D_F is the fractal dimension of the gel. These stronger effective molecular weight dependences do not indicate in any obvious manner the existence of qualitatively different mechanisms of polymer transport but emerge as natural generalizations of the constraint porosity effects predicted by PMC theory also for polymer melts and solutions. Indeed, this is a very important point applicable to all our new results. Traditionally, a change in N-scaling exponents is interpreted in terms of a new dominant transport mechanism at the level of individual polymer trajectories. In contrast, PMC theory focuses on the entanglement friction, and the diversity of possible scaling laws emerge as a consequence of the influence of structure and multiple competing length scales and relaxation channels on fluctuating force−time correlations. Real space physical motions do not need to be guessed as in phenomenological theories, nor can we unambiguously infer them.

In the following paper these theoretical predictions will be tested by quantitative comparisons with experimental data. A necessary preliminary is the estimation of the equilibrium parameters specifying the dynamics that will be accomplished using integral equation theories, computer simulation results, and experimental scattering and rheological data.

Acknowledgment. Partial financial support by the Deutsche Forschungsgemeinschaft under grant Fu 309/1-1, and the United States National Science Foundation MRSEC program via grant number NSF-DMR-89-20538, are gratefully acknowledged.

References and Notes

(1) Ferry, J. D. *Viscoelastic Properties of Polymers*; Wiley: New York, 1980.

(2) de Gennes, P. G. *Scaling Concepts in Polymer Physics*; Cornell University Press: Ithaca, NY, 1979.
(3) Doi, M.; Edwards, S. F. *The Theory of Polymer Dynamics*; Oxford University Press: Oxford, U.K., 1986.
(4) de Gennes, P. G. *J. Chem. Phys.* **1971**, *55*, 572.
(5) Schweizer, K. S. *J. Chem. Phys.* **1989**, *91*, 5802.
(6) Schweizer, K. S. *J. Chem. Phys.* **1989**, *91*, 5822.
(7) Lodge, T. P.; Rotstein, N.; Prager, S. *Adv. Chem. Phys.* **1990**, *79*, 1.
(8) Nemoto, N.; Kojima, T.; Inoue, T.; Kishine, M.; Hirayama, T.; Kurata, M. *Macromolecules* **1989**, *22*, 3793.
(9) Nemoto, N.; Kishine, M.; Inoue, T.; Osaki, K. *Macromolecules* **1990**, *23*, 659.
(10) Nemoto, N.; Kishine, M.; Inoue, T.; Osaki, K. *Macromolecules* **1991**, *24*, 1648.
(11) Rotstein, N. A.; Lodge, T. P. *Macromolecules* **1992**, *25*, 1316.
(12) Arvanitidou, E.; Hoagland, D. *Phys. Rev. Lett.* **1991**, *67*, 1464.
(13) Green, P. F.; Mills, P. J.; Palmstrom, C. J.; Mayer, J. W.; Kramer, E. J. *Phys. Rev. Lett.* **1984**, *58*, 2145.
(14) Nemoto, N. In *Polymer Rheology and Processing*; Collyer, A. A., Utracki, L. A., Eds.; Elsevier Science Publishers Ltd.: London and New York, 1990; p 3.
(15) Graessley, W. W. *Adv. Polym. Sci.* **1982**, *47*, 68.
(16) Klein, J. *Macromolecules* **1978**, *11*, 852.
(17) Klein, J. *Macromolecules* **1986**, *19*, 105.
(18) Doi, M. *J. Polym. Sci., Polym. Lett.* **1981**, *19*, 265.
(19) Doi, M. *J. Polym. Sci., Polym. Phys. Ed.* **1983**, *21*, 667.
(20) Adachi, K.; Wada, T.; Kawamoto, T.; Kotaka, T. *Macromolecules* **1995**, *28*, 3588.
(21) Poh, B. T.; Adachi, K.; Kotaka, T. *Macromolecules* **1996**, *29*, 6317.
(22) Fuchs, M.; Schweizer, K. S. *Macromolecules* **1997**, *30*, 5156 (following article in this issue).
(23) Flory, P. J. *Principles of Polymer Chemistry*; Cornell University Press: Ithaca, NY, 1953.
(24) Rouse, P. E. *J. Chem. Phys.* **1953**, *21*, 1272.
(25) Bixon, M.; Zwanzig, R. *J. Chem. Phys.* **1978**, *68*, 1896 and references cited therein.
(26) Hu, Y.; Macinnis, J. M.; Cherayil, B. J.; Fleming, G. R.; Freed, K. F.; Perico, A. *J. Chem. Phys.* **1990**, *93*, 822.
(27) Kawasaki, K. *Mod. Phys. Lett.* **1990**, *B4*, 913.
(28) Schweizer, K. S. *J. Non-Cryst. Solids* **1991**, *131−133*, 643.
(29) Schweizer, K. S. *Phys. Scr.* **1993**, *T49*, 99.
(30) Schweizer, K. S.; Szamel, G. *Philos. Mag.* **1993**, *B71*, 783.
(31) Schweizer, K. S.; Szamel, G. *Trans. Theo. Stat. Phys.* **1995**, *24*, 947.
(32) Schweizer, K. S.; Szamel, G. *J. Chem. Phys.* **1995**, *103*, 1934.
(33) Schweizer, K. S.; Szamel, G. *Macromolecules* **1995**, *28*, 7543.
(34) Fuchs, M.; Schweizer, K. S. *J. Chem. Phys.* **1997**, *106*, 347.
(35) Hansen, J. P.; McDonald, I. R. *Theory of Simple Liquids*; Academic Press: London, 1986.
(36) Appel, M.; Fleischer, G.; Kärger, J.; Fujara, F.; Chang, I. *Macromolecules* **1994**, *27*, 4274.
(37) Zawada, J. A.; Fuller, G. G.; Colby, R. H.; Fetters, L. J.; Roovers, J. *Macromolecules* **1994**, *27*, 6851.
(38) Hess, W.; Klein, R. *Adv. Phys.* **1983**, *32*, 173.
(39) Kawasaki, K. *Phys. Rev.* **1966**, *150*, 291.
(40) Fixman, M. *J. Chem. Phys.* **1962**, *36*, 310.
(41) Boon, J. P.; Yip, S. *Molecular Hydrodynamics*; Wiley: New York, 1980.
(42) Götze, W.; Sjögren, L. *Rep. Prog. Phys.* **1992**, *55*, 241.
(43) Yip, S., Ed. *Special Issue Devoted to Relaxation Kinetics in Supercooled Liquids—Mode Coupling Theory and its Experimental Tests*; Vol. 24 of Transactions of Theoretical and Statistical Physics; Marcel Dekker, Inc.: New York, 1995.
(44) Schweizer, K. S.; Curro, J. G. *Phys. Rev. Lett.* **1987**, *58*, 246.
(45) Schweizer, K. S.; Curro, J. G. *Adv. Polym. Sci.* **1994**, *116*, 319.
(46) Schweizer, K. S.; Curro, J. G. *Adv. Chem. Phys.* **1997**, *98*, 1.
(47) Hohenberg, P. C.; Halperin, B. I. *Rev. Mod. Phys.* **1977**, *49*, 435.
(48) Fuchs, M.; Hofacker, I.; Latz, A. *Phys. Rev.* **1992**, *A45*, 898.
(49) Akcasu, Z.; Gurol, H. *J. Polym. Sci., Polym. Phys.* **1970**, *14*, 1.
(50) Baumgaertel, M.; Rosa, M. E. D.; Machado, J.; Masse, M.; Winter, H. H. *Rheol. Acta* **1992**, *31*, 75.
(51) Jackson, J.; Rosa, M. E. D.; Winter, H. H. *Macromolecules* **1994**, *27*, 2426.
(52) Kannaan, R.; Lodge, T. P. *Macromolecules* **1997**, *30*, 3694.
(53) Adachi, K.; Kotaka, T. *Macromolecules* **1985**, *18*, 466.
(54) Imanishi, Y.; Adachi, K.; Kotaka, T. *J. Chem. Phys.* **1988**, *89*, 7585.
(55) Adachi, K.; Yoshida, H.; Fukui, F.; Kotaka, T. *Macromolecules* **1990**, *23*, 3138.
(56) Frick, B.; Farago, B.; Richter, D. *Phys. Rev. Lett.* **1988**, *61*, 2465.
(57) Patterson, G. D. *Adv. Polym. Sci.* **1983**, *48*, 125.
(58) Brown, W.; Nicolai, T. *Macromol. Symp.* **1994**, *79*, 139 and references cited therein.
(59) Nicolai, T.; Brown, W.; Hvidt, S.; Heller, K. *Macromolecules* **1990**, *23*, 5088.
(60) de Gennes, P. G.; Brochard, F. *Macromolecules* **1977**, *10*, 1157.
(61) Brochard, F. *J. Phys. (Paris)* **1983**, *44*, 39.
(62) Zimm, B. H. *J. Chem. Phys.* **1956**, *24*, 269.
(63) Schweizer, K. S.; Curro, J. G. *Chem. Phys.* **1990**, *149*, 105.
(64) Fuchs, M. *Z. Phys. B*, in press.
(65) Semenov, A. N. *Physica* **1990**, *A166*, 263.
(66) Genz, U. *Macromolecules* **1994**, *27*, 3501.
(67) Ronca, G. *J. Chem. Phys.* **1983**, *79*, 1031.
(68) de Gennes, P. G. *J. Phys. (Paris)* **1981**, *42*, 735.
(69) des Cloizeaux, J. *J. Phys. I Fr.* **1993**, *3*, 1523.
(70) Fetters, L. J.; Lohse, D. J.; Richter, D.; Witten, T. A.; Zirkel, A. *Macromolecules* **1994**, *27*, 4639.
(71) Paul, W.; Binder, K.; Heermann, D. W.; Kremer, K. *J. Chem. Phys.* **1991**, *95*, 7726.
(72) de Gennes, P. G. *Macromolecules* **1976**, *9*, 587.
(73) Colby, R. H.; Rubinstein, M. *Macromolecules* **1990**, *23*, 2753.
(74) Colby, R. H.; Fetters, L. J.; Graessley, W. W. *Macromolecules* **1987**, *20*, 2226.
(75) Pearson, D. S. *Rubber Chem. Technol.* **1987**, *60*, 437.
(76) Schweizer, K. S.; Szamel, G. *J. Chem. Phys.*, to be submitted.
(77) Dullien, F. A. *Porous Media, Fluid Transport and Pore Structure*; Academic Press: New York, 1979.
(78) Baumgärtner, A.; Muthukumar, M. *Adv. Chem. Phys.* **1996**, *94*, 625.
(79) Andrews, A. T. *Electrophoresis*: *Theory, Techniques, and Biochemical and Clinical Applications*; Oxford University Press, Oxford, U.K., 1986.
(80) Horkay, F.; Hecht, A. M.; Geisslen, E. *Faraday Discuss.* **1995**, *101*, 159.
(81) Ferri, F.; Frisken, B. J.; Cannell, D. S. *Phys. Rev. Lett.* **1991**, *67*, 3626.
(82) Baumgärtner, A.; Muthukumar, M. *J. Chem. Phys.* **1987**, *87*, 3082.
(83) Muthukumar, M.; Baumgärtner, A. *Macromolecules* **1989**, *22*, 1937.
(84) Muthukumar, M.; Baumgärtner, A. *Macromolecules* **1989**, *22*, 1941.

MA970234B